

1

2 **Title: Robust IgM responses following vaccination are associated with prevention of**  
3 ***Mycobacterium tuberculosis* infection in macaques**

4

5 **Authors:** Edward B. Irvine<sup>1,2</sup>, Anthony O'Neil<sup>1</sup>, Patricia A. Darrah<sup>3</sup>, Sally Shin<sup>1</sup>, Alok Choudhary<sup>4</sup>,  
6 Wenjun Li<sup>5</sup>, William Honnen<sup>4</sup>, Smriti Mehra<sup>6</sup>, Deepak Kaushal<sup>7</sup>, Hannah Priyadarshini Gideon<sup>8</sup>, JoAnne  
7 L. Flynn<sup>8</sup>, Mario Roederer<sup>3</sup>, Robert A. Seder<sup>3</sup>, Abraham Pinter<sup>4</sup>, Sarah Fortune<sup>1,2†\*</sup>, and Galit Alter<sup>1†\*</sup>

8

9 **Affiliations:**

10 <sup>1</sup> Ragon Institute of MGH, MIT and Harvard; Cambridge, MA, USA.

11 <sup>2</sup> Harvard T.H. Chan School of Public Health; Boston, MA, USA.

12 <sup>3</sup> Vaccine Research Center, National Institute of Allergy and Infectious Diseases (NIAID), National  
13 Institutes of Health; Bethesda, MD, USA.

14 <sup>4</sup> Public Health Research Institute, New Jersey Medical School, Rutgers, The State University of New  
15 Jersey; Newark, NJ, USA.

16 <sup>5</sup> Department of Medicine, University of Massachusetts Medical School; Worcester, MA, USA.

17 <sup>6</sup> Division of Microbiology, Tulane National Primate Research Center; Covington, Louisiana, USA.

18 <sup>7</sup> Southwest National Primate Research Center, Texas Biomedical Research Institute; San Antonio, TX  
19 78245, USA.

20 <sup>8</sup> Department of Microbiology and Molecular Genetics and Center for Vaccine Research, University of  
21 Pittsburgh School of Medicine; Pittsburgh, PA, USA.

22 <sup>†</sup> These authors contributed equally to this work.

23 \* Correspondence: [sfortune@hsph.harvard.edu](mailto:sfortune@hsph.harvard.edu) (S.M.F.) and [GALTER@mgh.harvard.edu](mailto:GALTER@mgh.harvard.edu) (G.A.)

24

25 **Abstract:** Development of an effective tuberculosis (TB) vaccine has suffered from an incomplete  
26 understanding of the correlates of protection against *Mycobacterium tuberculosis* (*Mtb*). However, recent  
27 work has shown that compared to standard intradermal Bacille Calmette-Guerin (BCG) vaccination,  
28 intravenous (IV) BCG vaccination provides nearly complete protection against TB in rhesus macaques.  
29 While studies have focused on cellular immunity in this setting, the antibody response elicited by IV BCG  
30 vaccination remains incompletely defined. Using an agnostic antibody profiling approach, here we show  
31 that IV BCG drives superior antibody responses in the plasma and the bronchoalveolar lavage fluid (BAL).  
32 While IV BCG immunization resulted in the broad expansion of antibody titers and effector functions,  
33 surprisingly, IgM titers were among the strongest markers of reduced bacterial burden in the plasma and  
34 BAL of BCG immunized animals. Moreover, IgM immunity was also enriched among animals receiving  
35 protective vaccination with an attenuated *Mtb* strain. Finally, a LAM-specific IgM monoclonal antibody  
36 reduced *Mtb* survival *in vitro*. Collectively, these data highlight the potential importance of IgM responses  
37 as a marker and as a functional mediator of protection against TB.

38 **Main Text:**

39 **INTRODUCTION**

40 *Mycobacterium tuberculosis* (*Mtb*), the causative agent of tuberculosis (TB), was responsible for  
41 the death of an estimated 1.4 million individuals in 2019 (1). While TB is curable, the intensive antibiotic  
42 regimen coupled with the rise in antibiotic resistance has underscored the need for an efficacious vaccine  
43 to help mitigate the global TB epidemic. Bacille Calmette-Guérin (BCG), first introduced in 1921, is the  
44 current standard for TB vaccination (2). While BCG is effective at preventing severe forms of TB in young  
45 children, BCG is poorly and variably efficacious in preventing pulmonary TB in adults (3). Consequently,  
46 novel vaccines and vaccination strategies are urgently needed.

47 TB vaccine development has suffered from a lack of understanding of the determinants of  
48 immunity against *Mtb* infection. CD4+ T cell knock-out studies in mice (4, 5), CD4+ depletion and simian  
49 immunodeficiency virus infection studies in non-human primates (NHPs) (6–8), as well as human  
50 immunodeficiency virus infected human cohort studies (9), have all found increased rates of TB disease  
51 progression in the setting of low CD4+ T counts, pointing to a critical role for CD4+ T cells in controlling  
52 *Mtb* infection. However, efforts to generate vaccines that primarily leverage T cell immunity to drive  
53 protection against TB have been met with limited success.

54 The first large-scale TB vaccine clinical trial since BCG was the T<sub>H</sub>1-directed MVA-85A vaccine  
55 phase 2b trial (10). Despite the lack of efficacy of MVA-85A vaccination, a post-hoc correlates analysis  
56 of the study found Ag85A-specific IgG responses to be linked with reduced risk of TB disease (11),  
57 identifying humoral immunity as an unexpected negative correlate of TB disease risk. More recently, the  
58 M72/AS01<sub>E</sub> phase 2b TB vaccine trial in adults reported a 50% reduction in rates of progression to active  
59 TB (ATB) (12). While robust T cell immunity was observed following M72-vaccination, strong anti-M72-  
60 specific humoral immunity was also observed, as all vaccinees in the M72/AS01<sub>E</sub> group remained  
61 seropositive 36 months following vaccination (12, 13). Together, these human vaccination studies point

62 to the potential importance of both cellular and humoral immunity in vaccine-mediated protection against  
63 TB.

64 In addition to the promising efficacy signals that have begun to emerge in human TB vaccine  
65 studies (13, 14), intravenous (IV) BCG vaccination of non-human primates (NHPs) has been shown to  
66 provide robust protection against *Mtb* infection (15–20). Remarkably, IV BCG vaccination resulted in a  
67 100,000-fold reduction in lung bacterial burden compared with standard intradermal BCG vaccination,  
68 with six out of ten macaques demonstrating no detectable level of *Mtb* infection (20). In contrast, high-  
69 dose intradermal BCG and aerosol BCG vaccination regimens resulted in lung bacterial burden levels  
70 similar to those observed with standard intradermal BCG vaccination (20). IV BCG vaccinated rhesus  
71 macaques exhibited increased antigen-responsive CD4 and CD8 T cells systemically, and locally in the  
72 lung compared to the other vaccination groups (20). Concomitant with enhanced T cell responses, IV BCG  
73 vaccinated animals elicited stronger whole-cell lysate reactive antibody responses in the plasma and  
74 bronchoalveolar lavage (BAL) fluid (20). Yet, while broad differences in antibody responses across BCG  
75 vaccination groups were observed in this study, their antigenic targets, functional and anti-microbial  
76 activity, and relationship with *Mtb* burden were not defined.

77 Here we leveraged Systems Serology to investigate the antigen-specific humoral immune  
78 responses that uniquely evolve following IV BCG vaccination in rhesus macaques (21). We demonstrate  
79 that compared to standard intradermal BCG vaccination, high dose intradermal BCG vaccination and  
80 aerosol BCG vaccination, IV BCG vaccination elicits superior antigen-specific humoral immunity in the  
81 periphery, and was the only regimen to induce a robust, lung-compartmentalized antibody response  
82 capable of restricting *Mtb* growth *in vitro*. While IgG, IgA, and several Fc-receptor binding antibody  
83 subpopulations expanded selectively in the lungs of IV immunized animals, antigen-specific IgM titers  
84 were strongly associated with reduced bacterial burden in the BAL and plasma of animals immunized  
85 with IV BCG. IgM titers were also found to be a marker of protective immunity in rhesus macaques  
86 mucosally vaccinated with an attenuated *Mtb* strain (*Mtb*-Δ*sigH*) – an orthogonal vaccination strategy also

87 shown to protect rhesus macaques from lethal *Mtb* challenge (22). Finally, we show that a LAM-specific  
88 IgM monoclonal antibody reduced *Mtb* survival *in vitro*, suggesting that vaccine-induced IgM responses  
89 are plausible contributors to vaccine-induced protection against *Mtb*.

90 **RESULTS**

91 **IV BCG immunization drives higher and more durable plasma antigen-specific antibody titers**

92 Following IV BCG immunization, there was a marked increase in *Mtb* whole-cell lysate reactive IgG and  
93 IgA titers compared to BCG administration by other routes (20). However, in this first study, the antibody  
94 responses elicited by the different BCG vaccination strategies to distinct *Mtb* antigen targets were not  
95 assessed. Thus, we sought to determine whether particular antigen-specific antibody populations are  
96 differentially induced by different BCG vaccination strategies. Antibody levels to a panel of *Mtb* antigens  
97 were compared using a custom, multiplexed Luminex assay (23). The antigen panel included: purified  
98 protein derivative (PPD) – a heterogenous collection of *Mtb* proteins (24), lipoarabinomannan (LAM) – a  
99 critical cell wall glycolipid (25), HspX – a stress induced intracellular protein (26), as well as PstS1 and  
100 Apa – both cell membrane associated glycoproteins linked to host cell invasion (27, 28). Of note, each of  
101 these antigens are expressed by both BCG and *Mtb*. Plasma samples collected pre-vaccination, week 8  
102 post-vaccination, time of *Mtb* challenge (week 24), and post-infection (week 28) were analyzed, and fold  
103 change in antibody titer over pre-vaccination levels was calculated for each macaque at each timepoint.

104 Following immunization and prior to infection, antigen-specific IgG1 responses were detected in  
105 macaques across all vaccine arms. There were weak responses to all antigens in animals receiving standard  
106 ID BCG (Fig 1A). Conversely, those that received IV BCG vaccination displayed the largest increase in  
107 plasma IgG1 titers to nearly all tested antigens following vaccination. More specifically, PPD, LAM,  
108 PstS1, and Apa IgG1 titers in the IV BCG group were each significantly higher than those in the standard  
109 ID BCG group both at week 8 post-vaccination, and at the time of *Mtb* challenge (week 24 post-  
110 vaccination) (Fig 1A). The additional vaccination groups – high dose intradermal (ID<sub>high</sub>), aerosol (AE),  
111 and aerosol/intradermal (AE/ID) – trended towards higher IgG1 levels compared to the standard ID BCG  
112 group, though the differences were only significant for the ID<sub>high</sub> Apa-specific response (Fig 1A).

113 Antigen-specific IgA responses were also observed following vaccination across each of the  
114 experimental BCG vaccination groups, though the fold increases in IgA titer were not as prominent as

115 those for IgG1. IV BCG vaccinated macaques elicited significantly higher IgA titers to LAM and PstS1  
116 at week 8 post-vaccination and at the time of *Mtb* challenge compared to the standard ID BCG group,  
117 which did not generate a detectable increase in antigen-specific IgA titers to any of the antigens following  
118 vaccination (Fig 1B). Animals in the ID<sub>high</sub> group also elicited a significant increase in LAM IgA titers at  
119 week 8 post-vaccination (Fig 1B). However, minimal vaccine-induced plasma IgA responses to the  
120 additional antigens were detected in the other groups (Fig 1B).

121 Finally, antigen-specific IgM responses were detected in multiple experimental BCG vaccination  
122 groups, with IV and ID<sub>high</sub> vaccinated macaques mounting the strongest peripheral IgM responses to BCG  
123 vaccination. IV BCG vaccinated animals exhibited significantly higher LAM-, PstS1-, and Apa-specific  
124 IgM titers at week 8 following vaccination compared to the standard ID BCG group, while responses in  
125 the ID<sub>high</sub> group were not significantly different (Fig 1C). LAM IgM titers also trended higher at the time  
126 of challenge in the IV group, though the difference was no longer significant at this timepoint (Fig 1C).

127 Together, these data highlight peripheral differences in the antibody response to specific antigens  
128 induced by distinct BCG vaccination strategies. IV BCG immunized animals generated particularly high  
129 antigen-specific antibody levels in the plasma, with protein- and LAM-specific antibody responses  
130 persisting exclusively in IV immunized animals 24 weeks following vaccination, to the time of *Mtb*  
131 challenge. Further, standard ID BCG vaccination generated a weaker antigen-specific antibody response  
132 than the experimental vaccination regimens tested – each of which delivered a larger dose of BCG in  
133 addition to changing route – suggesting that altering both route and dose may result in enhanced peripheral  
134 humoral immune responses to BCG vaccination.

135

136 **IV BCG vaccination uniquely elicits a robust lung-compartmentalized antibody response**

137 We next aimed to profile the antigen-specific humoral immune response at the site of infection using  
138 bronchoalveolar lavage fluid (BAL) collected from each macaque pre-vaccination, week 4 post-  
139 vaccination, and week 16 post-vaccination – the final timepoint the BAL procedure was performed prior

140 to *Mtb* challenge. IV BCG vaccination uniquely elicited a robust antibody response in the airways  
141 following vaccination (Fig 2A – C). Specifically, IV BCG vaccinated animals mounted IgG1, IgA, and  
142 IgM responses in the BAL that were significantly higher than the standard ID BCG group at week 4 across  
143 all mycobacterial antigens tested (Fig 2A – C). The magnitude of the responses was particularly striking,  
144 with over 100-fold increases in antibody levels observed for some IV BCG vaccinated macaques (Fig 2A).  
145 Most antibody responses elicited were transient, with only statistically significant levels of LAM-, PstS1-  
146 , and Apa-specific antibodies detected in the BAL 16 weeks following vaccination. A small number of  
147 macaques in the ID<sub>high</sub>, AE, and AE/ID groups additionally generated detectable antibody titers in the  
148 BAL following BCG vaccination (Fig 2A – C). However, these responses were limited to one or two  
149 macaques in each group, and were substantially lower in magnitude than responses generated in IV BCG  
150 immunized animals (Fig 2A – C). These data indicate that IV BCG vaccination alone induced strong,  
151 lung-compartmentalized, antigen-specific humoral immune responses. These antibodies contracted, but  
152 persisted at detectable levels in IV immunized animals for at least 4 months following immunization.

153

154 **Antibodies from IV BCG vaccinated macaques mediate superior innate immune activation**

155 Beyond their ability to bind and recognize pathogens or pathogen-infected cells, antibodies are able to  
156 deploy the anti-microbial activity of the innate immune system via Fc:Fc-receptor engagement to control  
157 a wide range of microbes (29). Further, Fc $\gamma$  receptor (Fc $\gamma$ R) signaling is necessary for the optimal survival  
158 and bacterial containment of *Mtb* in mice (30). Thus, we next measured the Fc $\gamma$ R binding and functional  
159 capacity of plasma- and BAL-derived antibodies elicited in each BCG-vaccinated macaque to determine  
160 whether certain antibody Fc $\gamma$ R binding profiles and/or antibody effector functions selectively tracked with  
161 distinct BCG vaccination strategies.

162 In the plasma, the IV BCG group displayed a trend towards higher levels of Fc $\gamma$ R binding  
163 antibodies than the standard ID BCG group across nearly all antigens measured, including significantly  
164 increased PPD-, PstS1-, and Apa-specific Fc $\gamma$ R2A and Fc $\gamma$ R3A binding antibodies 8 weeks post-

165 vaccination (Fig 3A). Further, although Fc $\gamma$ R binding antibodies waned by the time of *Mtb* challenge  
166 across all vaccination groups, IV BCG vaccinated macaques maintained significantly higher levels of  
167 PPD- and PstS1-specific Fc $\gamma$ R2A and Fc $\gamma$ R3A binding antibodies close to the time of challenge,  
168 suggesting durable antibody functionality in this group (Fig 3A). To examine plasma antigen-specific  
169 antibody functionality, antibody-dependent phagocytosis by monocytes and neutrophils, as well as NK  
170 cell degranulation assays were performed. Each of these measurements were captured for LAM-specific  
171 antibodies, as each BCG vaccination regimen elicited detectable LAM-specific antibody titers in the  
172 plasma (Fig 1A – C). Antibodies from IV BCG vaccinated macaques induced the most potent antibody-  
173 dependent neutrophil phagocytosis, which was moderately, yet significantly higher than that observed in  
174 the standard ID BCG group at week 8 post-vaccination (Fig 3B). In contrast, limited differences were  
175 observed in LAM-specific antibody-dependent monocyte phagocytosis and antibody-dependent NK cell  
176 degranulation – a surrogate for antibody-dependent cellular cytotoxicity (ADCC) (31) – across the vaccine  
177 groups (Fig 3B).

178 In line with the elevated antibody levels observed in the BAL of IV BCG vaccinated macaques  
179 (Fig 2A – C), antibodies in the IV group demonstrated the highest levels of Fc $\gamma$ R binding (Fig 3C). IV  
180 BCG immunized animals generated significantly higher levels of LAM-specific Fc $\gamma$ R2A binding  
181 antibodies at week 4 post-vaccination (Fig 3C). In addition, antigen-specific Fc $\gamma$ R3A binding levels in the  
182 BAL were particularly robust in the IV vaccinated group, with IV macaques displaying significantly  
183 higher levels of Fc $\gamma$ R3A binding antibodies to PPD, LAM, PstS1, and Apa 4 weeks following vaccination  
184 (Fig 3C). LAM-, and PstS1-specific Fc $\gamma$ R3A binding antibody levels remained significantly higher at  
185 week 16 post-vaccination (Fig 3C). Furthermore, BAL-derived antibodies in the IV group demonstrated  
186 superior LAM-specific functional activity. Specifically, BAL-derived antibodies from IV BCG vaccinated  
187 animals exhibited a trend towards stronger antibody-dependent monocyte phagocytosis activity (Fig 3D).  
188 More strikingly, the IV BCG group demonstrated significantly higher antibody-dependent neutrophil  
189 phagocytosis and NK cell degranulation activity week 4 vaccination, with little functionality observed in

190 the other vaccination groups (Fig 3D). This activity returned to baseline in a majority of animals by week  
191 16 post-vaccination (Fig 3D).

192 Previous data have linked an enrichment of Fc $\gamma$ R3A binding and NK cell activating antibodies in  
193 the setting of LTBI, to enhanced intracellular *Mtb* killing in macrophages (32). Therefore, given the  
194 expansion of both of these humoral features particularly in the BAL of the IV immunized group 4 weeks  
195 post-vaccination, we next examined the anti-microbial activity of antibodies from each vaccination group  
196 in this context. Human monocyte-derived macrophages were infected with a live/dead reporter strain of  
197 *Mtb* (33), followed by the addition of pooled plasma or BAL from each BCG vaccination group. Plasma  
198 from the IV group did not drive significant *Mtb* restriction across either of the timepoints (Fig 3E).  
199 Conversely, the week 4 IV BCG BAL pool did drive moderate, yet significant intracellular *Mtb* restriction,  
200 whereas the ID<sub>high</sub> BCG BAL pool tended to enhance infection. These patterns were consistently observed  
201 across all tested macrophage donors (Fig 3F).

202 Taken together, these data highlight the induction of highly functional antibodies following IV  
203 BCG immunization in rhesus macaques. Further, the increases selectively observed in Fc $\gamma$ R3A binding,  
204 NK cell degranulation, and intracellular *Mtb* killing in the BAL were particularly salient given recent  
205 associations reported between both Fc $\gamma$ R3A binding, as well as NK cell activity, and improved *Mtb* control  
206 (32, 34).

207

#### 208 **Antigen-specific IgM titers in the plasma and BAL negatively correlate with *Mtb* burden**

209 A spectrum of bacterial burden was observed in the lungs of rhesus macaques across the BCG vaccinated  
210 groups at the time of necropsy (20). Thus, despite IV immunization clearly affording optimal bacterial  
211 control following *Mtb* challenge, we next aimed to define whether any antibody features exhibited a robust  
212 relationship with lung *Mtb* burden.

213 In the plasma, 5 antibody measurements were significantly negatively associated with *Mtb* burden  
214 after multiple hypothesis testing correction (Fig 4A) (35). Surprisingly, each of the features identified

215 were antigen-specific IgM titers at week 8 post-vaccination or at the time of challenge (Fig 4A and B),  
216 revealing an unexpected significant relationship between plasma antigen-specific IgM titers and improved  
217 outcome following *Mtb* challenge. In contrast, while higher antibody titers have historically been  
218 associated with elevated antigenic burden and enhanced *Mtb* disease, antibody levels and features were  
219 not identified that tracked positively with *Mtb* burden at either significance level (Fig 4A).

220 In the BAL, 18 antibody features were significantly negatively associated with *Mtb* burden after  
221 multiple hypothesis testing correction (Fig 4C) (35). Several antigen-specific IgG1, IgA, IgM, and Fc $\gamma$ R  
222 binding measurements in the BAL at 4 or 16 weeks post-vaccination were negatively correlated with *Mtb*  
223 levels at the time of necropsy (Fig 4C and D). The majority of these features associated with reduced *Mtb*  
224 bacterial burden included antibody features present week 4 post-vaccination, the exception being LAM  
225 and PstS1 IgM titers at week 16 (Fig 4C and D). Again, none of the BAL antibody features measured had  
226 a significant positive correlation with *Mtb* burden at necropsy at either significance level (Fig 4C).

227 Collectively, the particularly low *Mtb* burden present in IV immunized animals indicate that the  
228 relationship observed between select humoral features and bacterial burden track with vaccination route,  
229 and thus may not represent independent correlates of protection. Nevertheless, these analyses point to the  
230 vaccine-induced humoral immune features which track most closely with improved microbial control in  
231 this vaccination cohort. Notably, IgM responses alone tracked with reduced *Mtb* burden close to the time  
232 of challenge across both compartments, potentially representing direct mechanistic correlates of  
233 immunity, or markers of a unique functional humoral immune response in these animals.

234

### 235 **Antibody profiles accurately distinguish protected and susceptible BCG-vaccinated macaques**

236 Given that many antibody titer and functional measurements were highly correlated, even across  
237 compartments, we next sought to determine whether a minimal set of antibody features could be defined  
238 that collectively tracked with *Mtb* control. Thus, macaques with a lung *Mtb* burden at necropsy below  
239 1000 were categorized as protected (total n = 11; 9 IV BCG, 1 ID<sub>high</sub>, 1 AE/ID BCG), and those with an

240 *Mtb* burden greater than or equal to 1000 were categorized as susceptible (total n = 37). Next, least absolute  
241 shrinkage and selection operator (LASSO) regularization was implemented on the standardized antibody  
242 data, removing variables unrelated to the outcome, as well as reducing the number of highly correlated  
243 features (36). Partial least squares discriminant analysis (PLS-DA) was then performed to visualize and  
244 quantify group separation (37, 38).

245 Robust separation was observed between protected and susceptible macaques on the basis of  
246 humoral profile (Fig 4E). The model distinguished protected from susceptible animals with a balanced  
247 cross-validation accuracy of 89.6% (Fig 4E). Remarkably, only 3 features were required to achieve this  
248 high level of predictive accuracy: BAL HspX-specific IgM at week 4, plasma LAM-specific IgG1 at week  
249 8, and plasma LAM-specific IgM at the time of challenge. Each of these features contributed to separation  
250 along latent variable 1 (LV1) (Fig 4F). The selection of these three variables across distinct timepoints  
251 suggests that substantive humoral differences were present between protected and susceptible BCG-  
252 vaccinated macaques beginning in the lung in week 4, extending out to the time of challenge in the plasma.  
253 Further, this analysis demonstrates that protected and susceptible BCG-vaccinated macaques can be  
254 accurately resolved by simply using antibody titer measurements.

255

## 256 **Protective vaccination via attenuated *Mtb* is associated with increased plasma IgM titers**

257 While our analyses identified humoral features associated with reduced *Mtb* burden in BCG immunized  
258 animals, because vaccination route was so closely linked to protection in this cohort, the generalizability  
259 of these findings was unclear. Thus, we next queried whether similar humoral features were associated  
260 with *Mtb* control in an independent *Mtb* vaccination study in NHPs. Previous work demonstrated that AE  
261 vaccination with an attenuated *Mtb* strain (*Mtb*-ΔsigH) provided superior protection compared to AE BCG  
262 vaccination in rhesus macaques (22). Thus, antibody profiling was performed on the plasma of *Mtb*-ΔsigH  
263 or AE BCG vaccinated animals.

264       Using antibody titer measurements alone, *Mtb-ΔsigH* and BCG vaccination groups could be  
265       clearly separated using a principal component analysis (PCA) (Fig 5A). Analysis of the PCA loadings plot  
266       revealed that antigen-specific IgM responses primarily drove separation between the two groups, with  
267       antigen-specific IgM responses enriched among protected *Mtb-ΔsigH* vaccinated macaques (Fig 5B).  
268       Similarly, univariate analyses indicated that *Mtb-ΔsigH* vaccinated macaques elicited significantly higher  
269       LAM-specific IgM titers week 7 post-vaccination, as well as a trend towards increased Apa- and HspX-  
270       specific IgM titers (Fig 5C). In contrast, minimal differences in antigen-specific IgG1 and IgA titers were  
271       noted between the *Mtb-ΔsigH* and BCG groups (Fig S4). Finally, antibody responses to the Ebola virus  
272       negative control antigen were not detected in either group as expected regardless of isotype (Figs 5C and  
273       S4).

274       Thus, although the sample size from this cohort is small, increased plasma antigen-specific IgM  
275       titers tracked with reduced *Mtb* disease. A result similar to that observed in BCG immunized animals (Fig  
276       4A), potentially hinting at a common association between antigen-specific IgM and vaccine-induced *Mtb*  
277       control.

278

### 279       **Superior *in vitro* anti-microbial effect of LAM-specific IgM**

280       Data from both the BCG route and the *Mtb-ΔsigH* immunization study pointed to an unexpected  
281       association of antigen-specific IgM titers with improved vaccine-induced *Mtb* control. However, whether  
282       elevated IgM levels represented a biomarker or contributed directly to anti-microbial control remained  
283       unclear. Given the emerging data pointing to an anti-microbial role for polyclonal IgG and monoclonal  
284       IgG and IgA antibodies against *Mtb* (32, 39–44), we next queried whether IgM also might harbor some  
285       anti-microbial capacity, using an engineered high-affinity LAM-specific antibody clone (A194) generated  
286       as an IgG1 and as an IgM (45).

287       In light of the previous observation that IgG1- and IgM-rich BAL from IV immunized rhesus  
288       macaques could drive intracellular *Mtb* killing in macrophages (Fig 3F), we first compared the anti-

289 microbial activity of each isotype in a similar human monocyte-derived macrophage model. However,  
290 despite the anti-microbial signal observed in the BAL of IV BCG immunized animals, neither LAM-  
291 specific monoclonal antibody drove significant intracellular *Mtb* restriction in macrophages when added  
292 post-infection (Fig 6A).

293 While macrophages represent a primary cellular niche for *Mtb* *in vivo* during infection, we also  
294 probed the anti-microbial role for each LAM-specific antibody in a whole-blood model of infection – a  
295 system which queries the broader role of multiple immune cell types and components in microbial  
296 restriction. Specifically, fresh blood from healthy human donors was simultaneously infected with an *Mtb*  
297 luciferase reporter strain (46), and treated with each LAM-specific monoclonal antibody. Luminescence  
298 readings were then taken to obtain *Mtb* growth curves in the presence of each antibody treatment over the  
299 course of 120 hours. Remarkably, only the LAM-specific IgM antibody drove significant *Mtb* restriction  
300 in this system (Fig 6B). Further, the LAM-specific IgM antibody drove improved bacterial restriction  
301 compared to the IgG1 across nearly every donor tested (Fig 6B).

302 Ultimately, these data demonstrate that a high-affinity LAM-specific antibody clone drives  
303 improved *Mtb* restriction in whole-blood as an IgM, as compared an IgG1 variant, suggesting that in  
304 addition to representing an early marker of vaccine-induced *Mtb* control, *Mtb*-specific IgM antibodies  
305 have the potential to functionally contribute to immunologic control of *Mtb*.

306 **DISCUSSION**

307 Recently, IV BCG vaccination in rhesus macaques was shown to result in robust protection against  
308 *Mtb* challenge (20), providing a unique opportunity to interrogate immunologic correlates and  
309 mechanisms of protection against *Mtb*. While published data highlighted the robust T cell immunity  
310 observed following IV BCG immunization, strong *Mtb* whole-cell lysate reactive humoral immune  
311 responses were also noted following this distinct vaccine delivery strategy (20). Given our emerging  
312 appreciation for a potential role for humoral immunity in *Mtb* control (47), here we deeply probed the  
313 antigen-specific humoral immune response across multiple BCG vaccine routes and doses to determine  
314 whether specific humoral immune profiles may complement cellular immunity, and potentially contribute  
315 to the protection afforded by IV BCG. Elevated antigen-specific antibody titers were observed in both the  
316 plasma and the lungs of IV BCG vaccinated animals, with a significant expansion of functional and anti-  
317 microbial responses in the BAL. Unexpectedly, correlation analyses revealed the unique association of  
318 BAL and plasma IgM responses close to or at the time of challenge, with reduced *Mtb* burden at necropsy  
319 in BCG immunized animals. Moreover, expanded plasma IgM titers were also observed in macaques  
320 immunized with an orthogonal, attenuated *Mtb* strain (*Mtb*-*ΔsigH*) that also conferred enhanced control  
321 over *Mtb* (22). Finally, a LAM-specific IgM antibody resulted in enhanced restrictive activity of *Mtb* *in*  
322 *vitro* compared to the same antibody clone with an IgG1 heavy chain, collectively pointing to a potential  
323 role for *Mtb*-specific IgM as a novel mechanistic correlate of protection in vaccine-induced *Mtb* control.

324 IV BCG immunized animals generated the strongest and most durable peripheral antibody  
325 responses directed to both protein antigens and to LAM. Conversely, standard ID BCG vaccination  
326 generated weaker antibody responses than the experimental vaccination regimens tested – each of which  
327 administered a larger dose of BCG (Fig 1). This pattern suggests that increased peak antibody titers may  
328 be a consequence of larger BCG dose delivered to these animals during immunization. However, each  
329 type of vaccination included in this study – intradermal, aerosol, and IV – additionally resulted in a distinct  
330 anatomic localization of vaccine antigen, where IV immunization resulted in robust localization in the

331 spleen (20), a primary site of B cell activation (48). Thus, it is conceivable that an enrichment of antigen  
332 particularly in this primary B cell inductive site, may contribute to the strong and long-lasting peripheral  
333 humoral immunity uniquely observed in IV BCG immunized animals.

334 Peripheral antibody titers, often of the IgG isotype, represent a primary correlate of protection for  
335 the majority of approved vaccines (47, 49–55). Yet surprisingly, vaccine-specific IgM titers were the only  
336 plasma antibody features to correlate inversely with *Mtb* burden in BCG immunized animals (Fig 4).  
337 Because protection was so dominantly associated with vaccination regimen, IgM titers did not represent  
338 an independent correlate of protection in the BCG route study. However, the potential value of IgM as a  
339 mechanistic correlate of immunity was corroborated by an enrichment in plasma IgM responses in animals  
340 that demonstrated enhanced *Mtb* control following *Mtb-ΔsigH* immunization (22). IgM plays a critical  
341 role during infection – particularly in the defense against other encapsulated bacteria – efficiently capable  
342 of driving phagocytosis, agglutination, and complement activation (56, 57). IgM has also been recently  
343 implicated as a critical regulator of T cell immune responses (58), raising the prospect of both direct anti-  
344 microbial, and indirect cellular regulatory roles for IgM in immunity against *Mtb*.

345 In the present study, we observed that a high-affinity LAM-specific antibody exhibited superior  
346 anti-microbial activity in primary human whole-blood as an IgM compared to as an IgG1. Unlike IgM  
347 antibodies that are elicited by vaccination or infection, this IgM monoclonal was an engineered form of a  
348 relatively high affinity IgG antibody (A194-01) (45, 59–61). While it is unclear whether IgM antibodies  
349 following IV BCG or *Mtb-ΔsigH* immunization require a similarly high affinity to drive anti-microbial  
350 function, the *in vitro* anti-microbial impact of this monoclonal suggests that IgM may not only serve as a  
351 surrogate of protective vaccine-induced immunity against *Mtb*, but may also play an unexpected  
352 mechanistic role in combating *Mtb* infection. Interestingly, several IgM LAM-specific monoclonal  
353 antibodies have been isolated from TB patients that also bind with moderate affinities, but not when  
354 expressed with an IgG heavy chain (45), suggesting that the increase in avidity provided by multimeric  
355 IgM may allow the antibody to access epitopes or drive Fc-mediated functions key to protective humoral

356 immunity. Notwithstanding, future work should continue to dissect the mechanistic basis for this *Mtb*  
357 restriction activity – including Fab- and Fc-mediated mechanisms through which IgM may contribute to  
358 protection.

359 Beyond superior plasma antibody responses, IV BCG immunization was uniquely associated with  
360 a significant increase in BAL IgG1, IgA, and IgM antibody titers to all mycobacterial antigens tested at  
361 week 4 post-vaccination. Despite the highly functional nature of the BAL-derived antibodies following  
362 IV BCG vaccination, it remains unclear whether enhanced antibody titers and functions present in the  
363 BAL represent a signature of protection, a signature of IV vaccination, or both. Follow-up studies, using  
364 reduced dosing of IV BCG, may provide critical clues required to uncover the quantitative and qualitative  
365 correlates of immunity against *Mtb*. However, rhesus macaques vaccinated with repeated low-dose  
366 endobronchial instillation of BCG exhibited increased protection against *Mtb* challenge compared to  
367 macaques vaccinated with standard ID BCG (62). These protected animals exhibited significantly higher  
368 PPD-specific antibody titers in the BAL compared to animals that received intradermal BCG  
369 immunization. While only PPD-specific IgA and PPD-specific pan-isotype antibodies were measured,  
370 these results point again to robust lung-residing humoral immune responses as a common immune  
371 signature of protection between these two studies and across vaccination strategies. Notably, both  
372 intravenous and endobronchially instilled BCG have been shown to drive substantial BCG deposition in  
373 the lungs (20). As such, it is possible that the localization of vaccine antigen deep in lungs – rather than  
374 in the dermis by ID vaccination, or in the upper respiratory tract by AE vaccination – may be critical for  
375 the induction of robust, lung-specific T and B cell immunity, that may work together to interrupt infection.

376 Lastly, despite the potent lung antibody responses observed in IV BCG immunized animals, the  
377 BAL antibody titers, functionality, and anti-microbial activity were largely transient (Figs 2 and 3). Thus,  
378 unlike lung T cell responses, which remained expanded over the course of the entire vaccination study  
379 (20), antibodies were less abundant in the lungs at the time of *Mtb* challenge (week 24). Critically, while  
380 differences may exist between BAL-derived antibodies and those found in the lung parenchyma, select

381 antibody features – including LAM-specific IgG1, IgA, IgM titers, and LAM-specific Fc $\gamma$ R3A binding  
382 antibodies – remained detectable and significantly higher in the airways of the IV group close to challenge.  
383 Given the small number of bacteria used in challenge (10 CFUs) (20), as well as the limited number of  
384 bacteria believed to cause infection in humans (63), it is plausible that even low levels of antibodies at the  
385 site of infection may be sufficient to capture the pathogen and contribute to first line defense. Of note,  
386 work in the context of influenza has demonstrated that vaccine-induced lung-resident memory B cell cells  
387 – particularly IgM+ memory B cells – may also play a critical role in rapid response to infection, swiftly  
388 generating antibody-secreting cells that rapidly re-populate the lung with antibodies able to control and  
389 clear infection (64, 65). Thus, it is conceivable that antibodies present in the airways 4 weeks post-  
390 vaccination, mark the establishment of lung-resident B cell immunity, which could respond  
391 instantaneously to *Mtb* challenge and contribute to protection in coordination with lung-resident T cell  
392 responses.

393 Ultimately, taken together, this work illustrates that IV BCG immunization drives superior plasma  
394 and lung antibody responses compared to ID and AE BCG vaccination. Specific humoral features  
395 associated with protection were identified across studies, highlighting potentially conserved roles for  
396 antibodies in vaccine-mediated protection against *Mtb*. Because of the potential safety issues associated  
397 with IV immunization, the development of alternative vaccination strategies able to mimic the protective  
398 humoral immune responses identified herein, may obviate the need for IV immunization to drive  
399 protection against TB in human populations. Thus, while efforts to leverage the immune response to  
400 combat TB via vaccination have largely focused on cellular immunity, this work demonstrates the value  
401 of a comprehensive examination of antibody characteristics across TB vaccine platforms, and motivates  
402 the continued study of antibodies as markers, and as functional mediators of protection against TB.

403 **MATERIALS AND METHODS**

404 **Study design**

405 Rhesus macaque (*Macaca mulatta*) plasma and bronchoalveolar lavage fluid (BAL) samples from the  
406 BCG route vaccination cohort were collected during a study performed at the Vaccine Research Center at  
407 the National Institutes of Health (20). All experimentation and sample collection from the original study  
408 complied with ethical regulations at the respective institutions (20). 48 BCG immunized animals were  
409 included in the study including: 10 animals that received standard intradermal (ID) BCG vaccination  
410 (target dose:  $5 \times 10^5$  CFUs), 8 animals that received high-dose intradermal (ID<sub>high</sub>) BCG vaccination  
411 (target dose:  $5 \times 10^7$  CFUs), 10 animals that received intravenous (IV) BCG vaccination (target dose:  $5 \times$   
412  $10^7$  CFUs), 10 animals that received aerosol (AE) BCG vaccination (target dose:  $5 \times 10^7$  CFUs), and 10  
413 animals that received a combination of AE and standard ID (AE/ID) BCG vaccination (target dose: AE  $5$   
414  $\times 10^7$  CFUs, ID  $5 \times 10^5$  CFUs) (20). Following BCG vaccination, each macaque was challenged with 10  
415 CFUs of *Mtb Erdman*, with a study endpoint of 12 weeks following *Mtb* challenge (20). In this study, *Mtb*  
416 burden values used throughout represent total thoracic CFUs measured at necropsy in the original study,  
417 and were measured as described previously (20). Plasma samples were analyzed from the following  
418 timepoints: pre-vaccination, week 8 post BCG vaccination, time of challenge (week 24 post BCG  
419 vaccination), and week 28 (4 weeks post *Mtb* challenge). BAL samples were analyzed from the following  
420 timepoints: pre-vaccination, week 4 post BCG vaccination, and week 16 post BCG vaccination. BAL was  
421 received as a 10X concentrate, and further diluted for experiments.

422 Rhesus macaque plasma samples from the attenuated *Mtb* vaccination cohort were collected during  
423 a study performed at the Tulane National Primate Research Center (22). All experimentation and sample  
424 collection from the original study were approved by the Institutional Animal Care and Use Committee  
425 and were performed in strict accordance with National Institutes of Health guidelines (22). Plasma from  
426 9 rhesus macaques were analyzed in the present study. 4 animals received AE BCG vaccination (target  
427 dose: 1,000 CFUs), and 5 animals received AE *Mtb-ΔsigH* – an attenuated *Mtb* strain in the CDC1551

428 genetic background – vaccination (target dose: 1,000 CFUs). Eight weeks post-vaccination, each animal  
429 was challenged with a target dose of 1,000 CFUs of *Mtb* *CDC1551* (22). Plasma samples were analyzed  
430 from the following timepoints: pre-vaccination, week 7 post-vaccination, and necropsy (week 15).

431

### 432 **Antigens**

433 To profile humoral immune responses, a panel of BCG/*Mtb*-antigens were used: purified protein  
434 derivative (PPD) (Statens Serum Institute), HspX (provided by T. Ottenhoff), LAM (BEI Resources, NR-  
435 14848), PstS1 (BEI Resources, NR-14859), and Apa (BEI Resources, NR-14862). Zaire ebolavirus  
436 glycoprotein (R&D Systems) was used as a negative control for the attenuated *Mtb* analysis.

437

### 438 **Non-human primate reagents**

439 Mouse anti-rhesus IgG1 (clone 7H11) and IgA (clone 9B9) secondary antibodies were obtained from the  
440 National Institutes of Health Nonhuman Primate Reagent Resource supported by AI126683 and  
441 OD010976. Mouse anti-monkey IgM (clone 2C11-1-5) was acquired from Life Diagnostics. Soluble  
442 rhesus macaque Fc $\gamma$ R2A and Fc $\gamma$ R3A were acquired from the Duke Human Vaccine Institute Protein  
443 Production Facility.

444

### 445 **Antigen-specific antibody levels**

446 Magnetic carboxylated fluorescent beads of distinct regions (Luminex Corp.) were first coupled to each  
447 protein antigen in a two-step carbodiimide reaction as described previously (23). LAM was modified by  
448 4-(4,6-dimethoxy[1,3,5]triazin-2-yl)-4-methyl-morpholinium (DMTMM) and coupled to Luminex  
449 magnetic carboxylated fluorescent beads using protocols described previously (66, 67).

450 Luminex using antigen-coupled beads to measure relative levels of antigen-specific antibodies was  
451 then performed as described previously (68), with minor modifications. A master mix of antigen-coupled  
452 beads was made at a concentration of 16.67 beads per  $\mu$ L per region in 0.1% bovine serum albumin (BSA)-

453 PBS, and 750 beads per region per well (45uL) were added to a clear, flat-bottom 384 well plate (Greiner).  
454 5uL of diluted sample was then added to the wells. Plasma from the BCG route vaccination study was  
455 diluted and run at 1:10 and 1:100. The 1:100 dilution was utilized for LAM IgG1, Apa IgG1, LAM IgA,  
456 and all IgM antigens. The 1:10 dilution was utilized for the remaining conditions. BAL from the BCG  
457 route vaccination study was diluted as follows: IgG1 1X, IgA 1X, IgM 0.1X. Plasma from the attenuated  
458 *Mtb* vaccination study was diluted as follows: IgG1 1:150, IgA 1:150, IgM 1:750. After adding the diluted  
459 samples, the plate was incubated shaking at 700 RPM overnight at 4°C. Next, the plate was washed 6  
460 times and 45uL of mouse anti-rhesus IgG1, IgA, or IgM antibody at 0.65ug/mL was added, and incubated  
461 shaking at 700 RPM at room temperature (RT) for 1 hour. The plate was then washed 6 times and 45uL  
462 of Phycoerythrin (PE)-conjugated goat anti-mouse IgG was added (ThermoFisher, 31861) and incubated  
463 shaking at 700RPM at RT for 1 hour. The plate was then washed 6 times, and resuspended in Sheath Fluid  
464 (Luminex Corp.) in a final volume of 60uL. PE median fluorescence intensity (MFI) levels were then  
465 measured via the FlexMap 3D (Luminex Corp.) Data are represented as fold change over pre-vaccination  
466 levels. Samples were measured in duplicate.

467

#### 468 **Antigen-specific Fc $\gamma$ receptor binding**

469 Rhesus macaque Fc $\gamma$ Rs were biotinylated as described previously (68). In brief, each Fc $\gamma$ R was  
470 biotinylated using a BirA biotin-protein ligase bulk reaction kit (Avidity) according to the protocol of the  
471 manufacturer, and excess biotin was removed using 3 kD cutoff centrifugal filter units (Amicon).

472 Luminex using biotinylated rhesus macaque Fc $\gamma$ Rs and antigen-coupled beads to measure relative  
473 binding levels of antigen-specific antibodies to Fc $\gamma$ Rs was then performed as described previously (68),  
474 with minor modifications. A master mix of antigen-coupled beads was made at a concentration of 16.67  
475 beads per  $\mu$ L per region in 0.1% BSA-PBS, and 750 beads per region per well (45uL) were added to a  
476 clear, flat-bottom 384 well plate (Greiner). 5uL of sample (Plasma: Fc $\gamma$ R2A 1:10, Fc $\gamma$ R3A 1:10; BAL:  
477 Fc $\gamma$ R2A 1X, Fc $\gamma$ R3A 1X) was added to the wells and incubated shaking at 700 RPM overnight at 4°C.

478 After overnight incubation, streptavidin-PE (ProZyme) was added to each biotinylated Fc $\gamma$ R in a 4:1 molar  
479 ratio and incubated rotating for 10 minutes at RT. 500 $\mu$ M biotin was then added at 1:100 relative to the  
480 total solution volume to quench the extra streptavidin-PE, and incubated rotating for 10 minutes at RT.  
481 After washing the assay plate 6 times, 40 $\mu$ L of each prepared detection Fc $\gamma$ R (1 $\mu$ g/ml in 0.1% BSA-PBS)  
482 was added to the immune-complexed microspheres and incubated shaking at 700 RPM for 1 hour at RT.  
483 The plate was then washed 6 times, and resuspended in Sheath Fluid (Luminex Corp.) in a final volume  
484 of 60 $\mu$ L. PE MFI levels were then measured via the FlexMap 3D (Luminex Corp.). Data represented as  
485 fold change over pre-vaccination level. Samples were measured in duplicate.

486

487 **Antibody-dependent cellular phagocytosis (ADCP)**

488 PPD ADCP (data not shown) was measured as described previously (32, 69). LAM ADCP was measured  
489 as described previously (32, 69) with minor changes. For every 100 $\mu$ g of LAM (dissolved in ddH<sub>2</sub>O),  
490 10 $\mu$ L of 1M sodium acetate (NaOAc), and 2.2 $\mu$ L of 50mM sodium periodate (NaIO<sub>4</sub>) was added. This  
491 oxidation reaction proceeded for 45 – 60min on ice in the dark. 12 $\mu$ L of 0.8M NaIO<sub>4</sub> was then added to  
492 block oxidation, and the solution was incubated for 5 min at RT in the dark. Next, the oxidized LAM was  
493 transferred to a new tube, and 10 $\mu$ L of 1M NaOAc and 22 $\mu$ L of 50mM hydrazide biotin (Sigma) were  
494 added. This biotinylation reaction proceeded for 2 hours at RT. Excess biotin was then removed using  
495 Amicon Ultra 0.5.L columns (3K, Millipore Sigma) according to the instructions of the manufacturer.  
496 Biotinylated LAM was then added to FITC-conjugated neutravidin beads (Invitrogen, 1.0 $\mu$ m) at a ratio of  
497 1 $\mu$ g antigen: 4 $\mu$ L beads, and incubated for overnight at 4°C. Excess antigen was washed away. Antigen-  
498 coated beads were incubated with 10 $\mu$ L of sample (plasma 1:10, BAL 1:1) for 2 hr at 37 °C. THP-1 cells  
499 (5  $\times$  10<sup>4</sup> per well) were added and incubated at 37 °C for 16 hr. Bead uptake was measured in fixed cells  
500 using flow cytometry on a BD LSRII (BD Biosciences) and analyzed by FlowJo 10.3. Phagocytic scores  
501 were calculated as: ((%FITC positive cells) x (geometric mean fluorescence intensity of the FITC positive

502 cells)) divided by 10,000. Data are represented as fold change over pre-vaccination levels. Samples were  
503 run in duplicate.

504

505 **Antibody-dependent neutrophil phagocytosis (ADNP)**

506 ADNP was performed as described previously (70), with minor changes. LAM was biotinylated and  
507 coupled to fluorescent neutravidin beads (1.0 $\mu$ m, Invitrogen), incubated with serum, and washed as  
508 described above for ADCP. During the 2-hour bead and serum incubation, fresh peripheral blood collected  
509 from healthy donors in acid citrate dextrose (ACD) anti-coagulant tubes was added at a 1:9 ratio to ACK  
510 lysis buffer (150mM NH<sub>4</sub>Cl, 8610mM KHCO<sub>3</sub>, 0.1mM Na<sub>2</sub>-EDTA, pH 7.4) for 5 minutes at RT. After  
511 red blood cell lysis, the blood was centrifuged for 5 minutes at 1500 RPM. After centrifugation,  
512 supernatant was removed, and leukocytes were washed with 50ml of 4°C PBS, spun for 5 minutes at 1500  
513 rpm and resuspended in R10 medium – (RPMI (Sigma), 10% fetal bovine serum (Sigma), 10mM HEPES  
514 (Corning), 2mM L-glutamine (Corning)) – at a final concentration of 2.5 x 10<sup>5</sup> cells/mL. Leukocytes (5 x  
515 10<sup>4</sup> cells/well) were then added to the immune-complexed beads and incubated for 1 hour at 37°C 5%  
516 CO<sub>2</sub>. Following this incubation, the plates were spun for 5 minutes at 500 x g. After removing the  
517 supernatant, anti-human CD66b-Pacific Blue (BioLegend) was added to the leukocytes, and the cells were  
518 incubated for 20 minutes at RT. Following this incubation, the cells were washed with PBS and fixed.  
519 Bead uptake was measured in fixed cells using flow cytometry on a BD LSRII (BD Biosciences) and  
520 analyzed by FlowJo 10.3. Phagocytic scores were calculated in the CD66b positive cell population. Data  
521 represented as fold change over pre-vaccination level. Samples were run in duplicate.

522

523 **Antibody-dependent NK cell activation (ADNKA)**

524 ADNKA was performed as described previously (32), with minor changes. ELISA plates (Thermo Fisher,  
525 NUNC MaxiSorp flat bottom) were coated with 150ng/well of LAM and incubated overnight at 4°C. The  
526 plates were then washed with PBS and blocked with 5% BSA-PBS for 2 hours. Next, the plates were

527 washed with PBS, and 50uL of sample (plasma 1:10, BAL 1X) was added and incubated for 2 hours at  
528 37°C. One day prior to adding the diluted sample, NK cells were isolated from healthy donors using the  
529 RosetteSep human NK cell enrichment cocktail (Stemcell) and Sepmate conical tubes (Stemcell)  
530 according to the instructions of the manufacturer. Following isolation, NK cells were incubated overnight  
531 at 1.5 x 10<sup>6</sup> cells/mL in R10 media with 1ng/mL human recombinant IL-15 (Stemcell). After the 2 hour  
532 serum incubation, the assay plates were washed, and 50,000 primary human NK cells, together with 2.5uL  
533 PE-Cy5 anti-human CD107a (BD), 0.4uL Brefeldin A (5mg/ml, Sigma), and 10uL GolgiStop (BD) were  
534 added to each well of the assay plates. The plates were then incubated for 5 hours at 37°C. Following the  
535 incubation, the samples from each well were stained with 1uL each of: PE-Cy7 anti-human CD56, APC-  
536 Cy7 anti-human CD16, and Alexa Fluor 700 anti-human CD3 (all from BD). After a 20 minute incubation  
537 at RT to allow extracellular staining, the plate was washed with PBS, and the cells were fixed using Perm  
538 A and Perm B (Invitrogen). The Perm B solution additionally contained PE anti-human MIP-1 $\beta$ , and APC  
539 anti-human IFN $\gamma$  (both from BD) to allow intracellular cytokine staining. After a final wash in PBS, the  
540 cells were resuspended in PBS and the fluorescence of each marker was measured on a BD LSR II flow  
541 cytometer (BD Biosciences) and analyzed by FlowJo 10.3. NK cells were defined as CD3 negative, CD16  
542 positive, CD56 positive cells. Data are represented as fold change over pre-vaccination levels. The assay  
543 was performed in biological duplicate using NK cells from 2 different donors.

544

#### 545 **Macrophage restriction assay (*Mtb*-live/dead)**

546 *In vitro* macrophage *Mtb* survival was measured as described previously (32), with minor changes. CD14  
547 positive cells were isolated from HIV negative donors using the EasySep CD14 Selection Kit II according  
548 to the instructions of the manufacturer (Stemcell). CD14 positive cells were matured for 7 days in R10  
549 media without phenol in low adherent flasks (Corning). Monocyte-derived macrophages (MDMs) were  
550 plated 50,000 cells per well in glass bottom, 96-well plates (Greiner) 24 hours prior to infection. A reporter  
551 *Mtb* strain (*Mtb*-live/dead) with constitutive mCherry expression and inducible green fluorescent protein

552 (GFP) expression (33), was cultured in log phase and filtered through a 5 $\mu$ m filter (Milliplex) prior to  
553 MDM infection at a multiplicity of infection of 1 for 14 hours at 37°C. Extracellular bacteria were washed  
554 off, and 200uL of pooled sample from each of the vaccination groups diluted in R10 without phenol  
555 (plasma 1:100, BAL 1X) was added. 3 days following infection, anhydrotetracycline (Sigma) (200 ng/ml)  
556 was added for 16 hours to induce GFP expression. 96 hours following infection, cells were fixed and  
557 stained with DAPI. Data were analyzed using the Columbus Image Data Storage and Analysis System.  
558 Bacterial survival was calculated as the ratio of live to total bacteria (the number of GFP+ pixels (live)  
559 divided by the number of mCherry+ pixels (total burden)) within macrophages in each well. Bacterial  
560 survival for each condition was normalized by bacterial survival in the no antibody condition. The assay  
561 was performed in technical triplicate using MDMs from 4 different donors.

562

### 563 **Macrophage restriction assay (*Mtb*-276)**

564 CD14 positive cells were isolated from HIV negative donors using the EasySep CD14 Selection Kit II  
565 according to the instructions of the manufacturer (Stemcell). CD14 positive cells were matured for 7 days  
566 in R10 media without phenol in low adherent flasks (Corning). MDMs were plated 50,000 cells per well  
567 in sterile, white, flat-bottom 96-well plate plates (Greiner) 24 hours prior to infection. An auto-luminescent  
568 *Mtb* reporter strain (*Mtb*-276) (46), was cultured in log phase and filtered through a 5 $\mu$ m filter (Milliplex)  
569 prior to MDM infection at a multiplicity of infection of 1, for 14 hours at 37°C. Extracellular bacteria  
570 were washed off, and each antibody treatment was diluted to 50ug/mL in R10 without phenol, and 200uL  
571 of diluted antibody was added to each MDM-containing well. Control treatments: rifampin (Sigma) at  
572 1ug/mL, human IgG1 isotype control (BE0297, BioXcell) at 50ug/mL, and human IgM isotype control  
573 (31146, Invitrogen) at 50ug/mL. Luminescence readings were then taken every 24 hours, up to 120 hours  
574 following infection to obtain *Mtb* growth curves in the presence of each antibody treatment. Area under  
575 the curve values were then computed for each antibody treatment in GraphPad Prism (version 8.4.0).

576

577 **Whole-blood restriction assay**

578 Whole-blood from HIV negative human donors was collected fresh the day of the experiment in acid  
579 citrate dextrose tubes. *Mtb*-276 previously cultured in 7H9 media at 37°C in log phase was washed once  
580 and resuspended in R10 media without phenol. Whole-blood was then infected with *Mtb*-276 such that  
581 the final concentration was 1x10<sup>6</sup> bacteria per mL of blood. Immediately after adding *Mtb*-276 to blood,  
582 150uL of blood and 150uL of antibody samples pre-diluted to 50ug/mL in R10 media are added together  
583 into a sterile, white, flat-bottom 96-well plate in triplicate (Greiner). Final concentration of experimental  
584 antibody treatments: 25ug/mL. Final concentration of control treatments: rifampin (Sigma) 0.25ug/mL,  
585 human IgG1 isotype control (BE0297, BioXcell) 25ug/mL, and human IgM isotype control (31146,  
586 Invitrogen) 25ug/mL. Samples in each well are mixed, then the first luminescence reading is taken on a  
587 plate reader (Tecan Spark 10M). The plate is then incubated at 37°C. Every 24 hours post-infection for  
588 120 hours, the samples in each well are mixed, and luminescence readings are taken on a plate reader to  
589 obtain *Mtb* growth curves in the presence of different antibody treatments. *Mtb* restriction in whole-blood  
590 is calculated as the area under the curve for each condition. Area under the curve values were computed  
591 for each antibody treatment in GraphPad Prism (version 8.4.0).

592

593 **LAM-specific monoclonal antibody expression**

594 A194 LAM-specific antibodies were generated as described previously (45). In brief, A194-IgG1 was  
595 generated by transfecting the A194-IGG1VH and IGVK plasmids into Expi293 cells. A194-IgM was  
596 generated by transfecting the A194-IGM1VH, IGVK, and joining (J) chain plasmids into Expi293 cells  
597 to generate multimeric IgM. Each antibody was purified by affinity chromatography. Protein A beads and  
598 protein L beads were used for the purification of IgG1 and IgM respectively. The antibodies were eluted  
599 using a low pH buffer, and characterized by SDS-PAGE for purity and size.

600

601 **Partial least squares discriminant analysis (PLS-DA)**

602 A multivariate model to distinguish protected and susceptible macaques was generated using a  
603 combination of least absolute shrinkage and selection operator (LASSO)-based feature selection (36, 71),  
604 and partial least squares discriminant analysis (PLS-DA) (37, 38). Protected macaques were defined as  
605 those with an *Mtb* burden less than 1000 CFU/mL at time of necropsy. *Mtb* burden values used represent  
606 total thoracic CFUs measured at necropsy in the original study, and were measured as described previously  
607 (20).

608 For feature selection, the data were z-scored and 100 bootstrap datasets were generated. A LASSO  
609 model in which the optimal penalty term lambda was chosen via 5-fold cross-validation, was then fit on  
610 each bootstrap dataset, and coefficients from each iteration of LASSO regularization were stored. Using  
611 these coefficients, variable inclusion probabilities – defined as the proportion of bootstrap replications in  
612 which a coefficient estimate is non-zero – were computed for each antibody feature. LASSO  
613 regularization was implemented using the *glmnet* package (version 3.0-2) in R (version 3.6.2).

614 PLS-DA models across a grid of variable inclusion probability cutoffs were fit in a 5-fold cross-  
615 validation framework repeated 100 times. Model accuracy – defined as ((1 – balanced error rate) x 100) –  
616 was computed for each. The optimal model, which contained 3 antibody features, was found at a variable  
617 inclusion probability of 0.45. A graph of the first and second latent variable (LV) from the optimal PLS-  
618 DA model is included, as is a variable importance in the projection (VIP) plot, indicating the relative  
619 contribution of individual features to separation along the first LV. The significance of the model was  
620 assessed using a permutation test. Specifically, the group labels of the macaques were randomly permuted.  
621 PLS-DA models were then fit and evaluated for model accuracy in a 5-fold cross-validation framework  
622 repeated 100 times. The accuracy of the real model was compared with that of the permuted model using  
623 a Mann-Whitney U test. PLS-DA models were implemented using the *mixOmics* package (version 6.10.9)  
624 in R (version 3.6.2).

625

626 **Statistics**

627 For the antibody titer (Fig 1 and 2), Fc $\gamma$ R binding (Fig 3 and S1), and functional measurements (Fig 3),  
628 from the BCG dose vaccination cohort, Kruskal-Wallis with Dunn's multiple-comparison tests were  
629 performed on the fold change values at each timepoint, comparing each vaccination group to the standard  
630 ID BCG group. For the macrophage *Mtb* restriction assay (Fig 3), a repeated measures ANOVA with  
631 Dunnett's multiple comparisons test was performed for each vaccination group, comparing pre-  
632 vaccination restrictive activity with that of each post-vaccination timepoint. For antibody titers in the  
633 attenuated *Mtb* vaccination cohort (*Mtb*- $\Delta$ *sigH*) (Fig 5 and S2), Mann-Whitney U tests were performed on  
634 the fold change values at each timepoint, comparing aerosol *Mtb*- $\Delta$ *sigH* to the aerosol BCG group. For  
635 the LAM-specific monoclonal antibody *Mtb* restriction assays, a repeated measures ANOVA with Sidak's  
636 multiple comparisons test was performed to make the relevant statistical comparisons. These statistics  
637 were performed in GraphPad Prism (version 8.4.0). Spearman correlations between *Mtb* burden and  
638 individual antibody features were computed in R (version 3.6.2) (Fig 4). Adjusted p-values (q-values)  
639 were calculated using the Benjamini-Hochberg procedure (35).

640

641

642

643

644

645

646

647

648

649

650

651

652 **REFERENCES**

653 1. World Health Organization, “WHO | Global Tuberculosis Report 2020” (2020).

654 2. World Health Organization, “Global Tuberculosis Report” (2019).

655 3. P. E. Fine, Variation in protection by BCG: implications of and for heterologous immunity. *Lancet*  
656 (*London, England*). **346**, 1339–45 (1995).

657 4. A. M. Caruso, N. Serbina, E. Klein, K. Triebold, B. R. Bloom, J. L. Flynn, Mice deficient in CD4  
658 T cells have only transiently diminished levels of IFN-gamma, yet succumb to tuberculosis. *J.*  
659 *Immunol.* **162**, 5407–16 (1999).

660 5. S. Yao, D. Huang, C. Y. Chen, L. Halliday, R. C. Wang, Z. W. Chen, CD4<sup>+</sup> T Cells Contain Early  
661 Extrapulmonary Tuberculosis (TB) Dissemination and Rapid TB Progression and Sustain  
662 Multieffector Functions of CD8<sup>+</sup> T and CD3<sup>-</sup> Lymphocytes: Mechanisms of CD4<sup>+</sup> T Cell  
663 Immunity. *J. Immunol.* **192**, 2120–2132 (2014).

664 6. P. L. Lin, T. Rutledge, A. M. Green, M. Bigbee, C. Fuhrman, E. Klein, J. L. Flynn, CD4 T cell  
665 depletion exacerbates acute *Mycobacterium tuberculosis* while reactivation of latent infection is  
666 dependent on severity of tissue depletion in cynomolgus macaques. *AIDS Res. Hum. Retroviruses*.  
667 **28**, 1693–702 (2012).

668 7. C. R. Diedrich, T. Rutledge, P. Maiello, T. M. Baranowski, A. G. White, H. J. Borish, P. Karel, F.  
669 Hopkins, J. Brown, S. M. Fortune, J. L. Flynn, Z. Ambrose, P. L. Lin, SIV and *Mycobacterium*  
670 tuberculosis synergy within the granuloma accelerates the reactivation pattern of latent  
671 tuberculosis. *PLOS Pathog.* **16**, e1008413 (2020).

672 8. C. R. Diedrich, J. T. Mattila, E. Klein, C. Janssen, J. Phuah, T. J. Sturgeon, R. C. Montelaro, P. L.  
673 Lin, J. A. L. Flynn, Reactivation of latent tuberculosis in cynomolgus macaques infected with SIV  
674 is associated with early peripheral T cell depletion and not virus load. *PLoS One.* **5** (2010),  
675 doi:10.1371/journal.pone.0009611.

676 9. H. Esmail, C. Riou, E. du Bruyn, R. P.-J. Lai, Y. X. R. Harley, G. Meintjes, K. A. Wilkinson, R. J.

677 Wilkinson, The Immune Response to *Mycobacterium tuberculosis* in HIV-1-Coinfected Persons.

678 *Annu. Rev. Immunol.* **36**, 603–638 (2018).

679 10. M. D. Tameris, M. Hatherill, B. S. Landry, T. J. Scriba, M. A. Snowden, S. Lockhart, J. E. Shea, J.

680 B. McClain, G. D. Hussey, W. A. Hanekom, H. Mahomed, H. McShane, MVA85A 020 Trial Study

681 Team, Safety and efficacy of MVA85A, a new tuberculosis vaccine, in infants previously

682 vaccinated with BCG: a randomised, placebo-controlled phase 2b trial. *Lancet (London, England)*.

683 **381**, 1021–8 (2013).

684 11. H. A. Fletcher, M. A. Snowden, B. Landry, W. Rida, I. Satti, S. A. Harris, M. Matsumiya, R.

685 Tanner, M. K. Oshea, V. Dheenadhayalan, L. Bogardus, L. Stockdale, L. Marsay, A. Chomka, R.

686 Harrington-Kandt, Z. R. Manjaly-Thomas, V. Naranbhai, E. Stylianou, F. Darboe, A. Penn-

687 Nicholson, E. Nemes, M. Hatheril, G. Hussey, H. Mahomed, M. Tameris, J. B. McClain, T. G.

688 Evans, W. A. Hanekom, T. J. Scriba, H. McShane, T-cell activation is an immune correlate of risk

689 in BCG vaccinated infants. *Nat. Commun.* **7** (2016), doi:10.1038/ncomms11290.

690 12. D. R. Tait, M. Hatherill, O. Van Der Meeren, A. M. Ginsberg, E. Van Brakel, B. Salaun, T. J.

691 Scriba, E. J. Akite, H. M. Ayles, A. Bollaerts, M.-A. Demoitié, A. Diacon, T. G. Evans, P. Gillard,

692 E. Hellström, J. C. Innes, M. Lempicki, M. Malahleha, N. Martinson, D. Mesia Vela, M. Muyoyeta,

693 V. Nduba, T. G. Pascal, M. Tameris, F. Thienemann, R. J. Wilkinson, F. Roman, Final Analysis

694 of a Trial of M72/AS01 E Vaccine to Prevent Tuberculosis . *N. Engl. J. Med.* **381**, 2429–2439

695 (2019).

696 13. O. Van Der Meeren, M. Hatherill, V. Nduba, R. J. Wilkinson, M. Muyoyeta, E. Van Brakel, H. M.

697 Ayles, G. Henostroza, F. Thienemann, T. J. Scriba, A. Diacon, G. L. Blatner, M.-A. Demoitié, M.

698 Tameris, M. Malahleha, J. C. Innes, E. Hellström, N. Martinson, T. Singh, E. J. Akite, A. Khatoon

699 Azam, A. Bollaerts, A. M. Ginsberg, T. G. Evans, P. Gillard, D. R. Tait, Phase 2b Controlled Trial

700 of M72/AS01E Vaccine to Prevent Tuberculosis. *N. Engl. J. Med.* **379**, 1621–1634 (2018).

701 14. E. Nemes, H. Geldenhuys, V. Rozot, K. T. Rutkowski, F. Ratangee, N. Bilek, S. Mabwe, L.

702 Makhethé, M. Erasmus, A. Toefy, H. Mulenga, W. A. Hanekom, S. G. Self, L.-G. Bekker, R. Ryall,  
703 S. Gurunathan, C. A. DiazGranados, P. Andersen, I. Kromann, T. Evans, R. D. Ellis, B. Landry, D.  
704 A. Hokey, R. Hopkins, A. M. Ginsberg, T. J. Scriba, M. Hatherill, C-040-404 Study Team,  
705 Prevention of *M. tuberculosis* Infection with H4:IC31 Vaccine or BCG Revaccination. *N. Engl. J.  
706 Med.* **379**, 138–149 (2018).

707 15. R. L. Anacker, W. Brehmer, W. R. Barclay, W. R. Leif, E. Ribi, J. H. Simmons, A. W. Smith,  
708 Superiority of intravenously administered BCG and BCG cell walls in protecting rhesus monkeys  
709 (Macaca mulatta) against airborne tuberculosis. *Z. Immunitätsforsch. Exp. Klin. Immunol.* **143**,  
710 363–76 (1972).

711 16. W. R. Barclay, W. M. Busey, D. W. Dalgard, R. C. Good, B. W. Janicki, J. E. Kasik, E. Ribi, C. E.  
712 Ulrich, E. Wolinsky, Protection of monkeys against airborne tuberculosis by aerosol vaccination  
713 with bacillus Calmette-Guerin. *Am. Rev. Respir. Dis.* **107**, 351–8 (1973).

714 17. W. R. Barclay, R. L. Anacker, W. Brehmer, W. Leif, E. Ribi, Aerosol-Induced Tuberculosis in  
715 Subhuman Primates and the Course of the Disease After Intravenous BCG Vaccination. *Infect.  
716 Immun.* **2**, 574–82 (1970).

717 18. E. Ribi, R. L. Anacker, W. R. Barclay, W. Brehmer, S. C. Harris, W. R. Leif, J. Simmons, Efficacy  
718 of mycobacterial cell walls as a vaccine against airborne tuberculosis in the Rhesus monkey. *J.  
719 Infect. Dis.* **123**, 527–538 (1971).

720 19. S. Sharpe, A. White, C. Sarfas, L. Sibley, F. Gleeson, A. McIntyre, R. Basaraba, S. Clark, G. Hall,  
721 E. Rayner, A. Williams, P. D. Marsh, M. Dennis, Alternative BCG delivery strategies improve  
722 protection against *Mycobacterium tuberculosis* in non-human primates: Protection associated with  
723 mycobacterial antigen-specific CD4 effector memory T-cell populations. *Tuberculosis (Edinb).*  
724 **101**, 174–190 (2016).

725 20. P. A. Darrah, J. J. Zeppa, P. Maiello, J. A. Hackney, M. H. Wadsworth, T. K. Hughes, S. Pokkali,  
726 P. A. Swanson, N. L. Grant, M. A. Rodgers, M. Kamath, C. M. Causgrove, D. J. Laddy, A. Bonavia,

727 D. Casimiro, P. L. Lin, E. Klein, A. G. White, C. A. Scanga, A. K. Shalek, M. Roederer, J. A. L.  
728 Flynn, R. A. Seder, Prevention of tuberculosis in macaques after intravenous BCG immunization.  
729 *Nature*. **577**, 95–102 (2020).

730 21. A. W. Chung, M. P. Kumar, K. B. Arnold, W. H. Yu, M. K. Schoen, L. J. Dunphy, T. J. Suscovich,  
731 N. Frahm, C. Linde, A. E. Mahan, M. Hoffner, H. Streeck, M. E. Ackerman, M. J. McElrath, H.  
732 Schuitemaker, M. G. Pau, L. R. Baden, J. H. Kim, N. L. Michael, D. H. Barouch, D. A.  
733 Lauffenburger, G. Alter, Dissecting Polyclonal Vaccine-Induced Humoral Immunity against HIV  
734 Using Systems Serology. *Cell*. **163**, 988–998 (2015).

735 22. D. Kaushal, T. W. Foreman, U. S. Gautam, X. Alvarez, T. Adekambi, J. Rangel-Moreno, N. A.  
736 Golden, A. M. F. Johnson, B. L. Phillips, M. H. Ahsan, K. E. Russell-Lodrigue, L. A. Doyle, C. J.  
737 Roy, P. J. Didier, J. L. Blanchard, J. Rengarajan, A. A. Lackner, S. A. Khader, S. Mehra, Mucosal  
738 vaccination with attenuated *Mycobacterium tuberculosis* induces strong central memory responses  
739 and protects against tuberculosis. *Nat. Commun.* **6** (2015), doi:10.1038/ncomms9533.

740 23. E. P. Brown, A. F. Licht, A.-S. Dugast, I. Choi, C. Bailey-Kellogg, G. Alter, M. E. Ackerman,  
741 High-throughput, multiplexed IgG subclassing of antigen-specific antibodies from clinical samples.  
742 *J. Immunol. Methods*. **386**, 117–23 (2012).

743 24. H. Yang, N. A. Kruh-Garcia, K. M. Dobos, Purified protein derivatives of tuberculin - past, present,  
744 and future. *FEMS Immunol. Med. Microbiol.* **66** (2012), pp. 273–280.

745 25. A. K. Mishra, N. N. Driessens, B. J. Appelmelk, G. S. Besra, Lipoarabinomannan and related  
746 glycoconjugates: structure, biogenesis and role in *Mycobacterium tuberculosis* physiology and  
747 host-pathogen interaction. *FEMS Microbiol. Rev.* **35**, 1126–57 (2011).

748 26. Y. Yuan, D. D. Crane, R. M. Simpson, Y. Q. Zhu, M. J. Hickey, D. R. Sherman, C. E. Barry, The  
749 16-kDa alpha-crystallin (Acr) protein of *Mycobacterium tuberculosis* is required for growth in  
750 macrophages. *Proc. Natl. Acad. Sci. U. S. A.* **95**, 9578–83 (1998).

751 27. M. Esparza, B. Palomares, T. García, P. Espinosa, E. Zenteno, R. Mancilla, PstS-1, the 38-kDa

752 Mycobacterium tuberculosis glycoprotein, is an adhesin, which binds the macrophage mannose  
753 receptor and promotes phagocytosis. *Scand. J. Immunol.* **81**, 46–55 (2015).

754 28. A. Ragas, L. Roussel, G. Puzo, M. Rivière, The Mycobacterium tuberculosis cell-surface  
755 glycoprotein apa as a potential adhesin to colonize target cells via the innate immune system  
756 pulmonary C-type lectin surfactant protein A. *A. J. Biol. Chem.* **282**, 5133–5142 (2007).

757 29. L. L. Lu, T. J. Suscovich, S. M. Fortune, G. Alter, Beyond binding: antibody effector functions in  
758 infectious diseases. *Nat. Rev. Immunol.* **18**, 46–61 (2018).

759 30. P. J. Maglione, J. Xu, A. Casadevall, J. Chan, Fc gamma receptors regulate immune activation and  
760 susceptibility during Mycobacterium tuberculosis infection. *J. Immunol.* **180**, 3329–38 (2008).

761 31. G. Alter, J. M. Malenfant, M. Altfeld, CD107a as a functional marker for the identification of  
762 natural killer cell activity. *J. Immunol. Methods.* **294**, 15–22 (2004).

763 32. L. L. Lu, A. W. Chung, T. R. Rosebrock, M. Ghebremichael, W. H. Yu, P. S. Grace, M. K. Schoen,  
764 F. Tafesse, C. Martin, V. Leung, A. E. Mahan, M. Sips, M. P. Kumar, J. Tedesco, H. Robinson, E.  
765 Tkachenko, M. Draghi, K. J. Freedberg, H. Streeck, T. J. Suscovich, D. A. Lauffenburger, B. I.  
766 Restrepo, C. Day, S. M. Fortune, G. Alter, A Functional Role for Antibodies in Tuberculosis. *Cell.*  
767 **167**, 433-443.e14 (2016).

768 33. C. J. Martin, M. G. Booty, T. R. Rosebrock, C. Nunes-Alves, D. M. Desjardins, I. Keren, S. M.  
769 Fortune, H. G. Remold, S. M. Behar, Efferocytosis is an innate antibacterial mechanism. *Cell Host  
770 Microbe.* **12**, 289–300 (2012).

771 34. R. Roy Chowdhury, F. Vallania, Q. Yang, C. J. Lopez Angel, F. Darboe, A. Penn-Nicholson, V.  
772 Rozot, E. Nemes, S. T. Malherbe, K. Ronacher, G. Walzl, W. Hanekom, M. M. Davis, J. Winter,  
773 X. Chen, T. J. Scriba, P. Khatri, Y. Chien, A multi-cohort study of the immune factors associated  
774 with M. tuberculosis infection outcomes. *Nature.* **560**, 644–648 (2018).

775 35. Y. Benjamini, Y. Hochberg, Controlling the False Discovery Rate: A Practical and Powerful  
776 Approach to Multiple Testing. *J. R. Stat. Soc. Ser. B.* **57**, 289–300 (1995).

777 36. J. Friedman, T. Hastie, R. Tibshirani, Regularization Paths for Generalized Linear Models via  
778 Coordinate Descent. *J. Stat. Softw.* **33**, 1–22 (2010).

779 37. F. Rohart, B. Gautier, A. Singh, K.-A. Lê Cao, mixOmics: An R package for 'omics feature  
780 selection and multiple data integration. *PLoS Comput. Biol.* **13**, e1005752 (2017).

781 38. L. C. Lee, C.-Y. Liong, A. A. Jemain, Partial least squares-discriminant analysis (PLS-DA) for  
782 classification of high-dimensional (HD) data: a review of contemporary practice strategies and  
783 knowledge gaps. *Analyst*. **143**, 3526–3539 (2018).

784 39. B. Hamasur, M. Haile, A. Pawlowski, U. Schroder, G. Kallenius, S. B. Svenson, A mycobacterial  
785 lipoarabinomannan specific monoclonal antibody and its F(ab') fragment prolong survival of mice  
786 infected with *Mycobacterium tuberculosis*. *Clin. Exp. Immunol.* **138**, 30–8 (2004).

787 40. R. Teitelbaum, A. Glatman-Freedman, B. Chen, J. B. Robbins, E. Unanue, A. Casadevall, B. R.  
788 Bloom, Howard, A mAb recognizing a surface antigen of *Mycobacterium tuberculosis* enhances  
789 host survival. *Microbiology*. **95**, 15688–15693 (1998).

790 41. K. Pethe, S. Alonso, F. Biet, G. Delogu, M. J. Brennan, C. Locht, F. D. Menozzi, The heparin-  
791 binding haemagglutinin of *M. tuberculosis* is required for extrapulmonary dissemination. *Nature*.  
792 **412**, 190–4 (2001).

793 42. S. Balu, R. Reljic, M. J. Lewis, R. J. Pleass, R. McIntosh, C. van Kooten, M. van Egmond, S.  
794 Challacombe, J. M. Woof, J. Ivanyi, A novel human IgA monoclonal antibody protects against  
795 tuberculosis. *J. Immunol.* **186**, 3113–9 (2011).

796 43. H. Li, X.-X. Wang, B. Wang, L. Fu, G. Liu, Y. Lu, M. Cao, H. Huang, B. Javid, Latently and  
797 uninfected healthcare workers exposed to TB make protective antibodies against *Mycobacterium*  
798 tuberculosis. *Proc. Natl. Acad. Sci. U. S. A.* **114**, 5023–5028 (2017).

799 44. E. Roy, E. Stavropoulos, J. Brennan, S. Coade, E. Grigorjeva, B. Walker, B. Dagg, R. E. Tascon,  
800 D. B. Lowrie, M. J. Colston, S. Jolles, Therapeutic efficacy of high-dose intravenous  
801 immunoglobulin in *Mycobacterium tuberculosis* infection in mice. *Infect. Immun.* **73**, 6101–9

802 (2005).

803 45. A. Choudhary, D. Patel, W. Honnen, Z. Lai, R. S. Prattipati, R. B. Zheng, Y.-C. Hsueh, M. L.  
804 Gennaro, A. Lardizabal, B. I. Restrepo, M. Garcia-Viveros, M. Joe, Y. Bai, K. Shen, K. Sahloul, J.  
805 S. Spencer, D. Chatterjee, T. Broger, T. L. Lowary, A. Pinter, Characterization of the Antigenic  
806 Heterogeneity of Lipoarabinomannan, the Major Surface Glycolipid of *Mycobacterium*  
807 tuberculosis , and Complexity of Antibody Specificities toward This Antigen . *J. Immunol.* **200**,  
808 3053–3066 (2018).

809 46. N. Andreu, A. Zelmer, T. Fletcher, P. T. Elkington, T. H. Ward, J. Ripoll, T. Parish, G. J. Bancroft,  
810 U. Schaible, B. D. Robertson, S. Wiles, Optimisation of bioluminescent reporters for use with  
811 mycobacteria. *PLoS One.* **5**, e10777 (2010).

812 47. J. M. Achkar, A. Casadevall, Antibody-Mediated Immunity against Tuberculosis: Implications for  
813 Vaccine Development. *Cell Host Microbe.* **13**, 250–262 (2013).

814 48. R. E. Mebius, G. Kraal, Structure and function of the spleen. *Nat. Rev. Immunol.* **5** (2005), pp. 606–  
815 616.

816 49. R. A. Mason, N. M. Tauraso, R. O. Spertzel, R. K. Ginn, Yellow fever vaccine: direct challenge of  
817 monkeys given graded doses of 17D vaccine. *Appl. Microbiol.* **25**, 539–44 (1973).

818 50. H. Faden, J. F. Modlin, M. L. Thoms, A. M. McBean, M. B. Ferdon, P. L. Ogra, Comparative  
819 evaluation of immunization with live attenuated and enhanced-potency inactivated trivalent  
820 poliovirus vaccines in childhood: systemic and local immune responses. *J. Infect. Dis.* **162**, 1291–  
821 7 (1990).

822 51. A. D. Jack, A. J. Hall, N. Maine, M. Mendy, H. C. Whittle, What Level of Hepatitis B Antibody Is  
823 Protective? *J. Infect. Dis.* **179**, 489–492 (1999).

824 52. L. H. Lee, C. E. Frasch, L. A. Falk, D. L. Klein, C. D. Deal, Correlates of immunity for  
825 pneumococcal conjugate vaccines. *Vaccine.* **21**, 2190–6 (2003).

826 53. I. Frazer, Correlating immunity with protection for HPV infection. *Int. J. Infect. Dis.* **11**, S10–S16

827 (2007).

828 54. S. A. Plotkin, Correlates of Protection Induced by Vaccination. *Clin. Vaccine Immunol.* **17**, 1055–  
829 1065 (2010).

830 55. A. K. Wheatley, S. J. Kent, Prospects for antibody-based universal influenza vaccines in the context  
831 of widespread pre-existing immunity. *Expert Rev. Vaccines.* **14**, 1227–1239 (2015).

832 56. M. R. Ehrenstein, C. A. Notley, The importance of natural IgM: scavenger, protector and regulator.  
833 *Nat. Rev. Immunol.* **10**, 778–86 (2010).

834 57. V. B. Klimovich, IgM and its receptors: Structural and functional aspects. *Biochem.* **76** (2011), pp.  
835 534–549.

836 58. A. Meryk, L. Pangrazzi, M. Hagen, F. Hatzmann, B. Jenewein, B. Jakic, N. Hermann-Kleiter, G.  
837 Baier, J. Jylhävä, M. Hurme, K. Trieb, B. Grubeck-Loebenstein, Fc $\mu$  receptor as a Costimulatory  
838 Molecule for T Cells. *Cell Rep.* **26**, 2681-2691.e5 (2019).

839 59. T. Broger, B. Sossen, E. du Toit, A. D. Kerkhoff, C. Schutz, E. Ivanova Reipold, A. Ward, D. A.  
840 Barr, A. Macé, A. Trollip, R. Burton, S. Ongarello, A. Pinter, T. L. Lowary, C. Boehme, M. P.  
841 Nicol, G. Meintjes, C. M. Denkinger, Novel lipoarabinomannan point-of-care tuberculosis test for  
842 people with HIV: a diagnostic accuracy study. *Lancet Infect. Dis.* **19**, 852–861 (2019).

843 60. G. B. Sigal, A. Pinter, T. L. Lowary, M. Kawasaki, A. Li, A. Mathew, M. Tsionsky, R. B. Zheng,  
844 T. Plisova, K. Shen, K. Katsuragi, A. Choudhary, W. J. Honnen, P. Nahid, C. M. Denkinger, T.  
845 Broger, A novel sensitive immunoassay targeting the 5-methylthio-D-xylofuranose–  
846 lipoarabinomannan epitope meets the WHO’s performance target for tuberculosis diagnosis. *J.  
847 Clin. Microbiol.* **56** (2018), doi:10.1128/JCM.01338-18.

848 61. T. Broger, M. P. Nicol, G. B. Sigal, E. Gotuzzo, A. J. Zimmer, S. Surtie, T. Caceres-Nakiche, A.  
849 Mantsoki, E. I. Reipold, R. Székely, M. Tsionsky, J. van Heerden, T. Plisova, K. Chikamatsu, T.  
850 L. Lowary, A. Pinter, S. Mitarai, E. Moreau, S. G. Schumacher, C. M. Denkinger, Diagnostic  
851 accuracy of 3 urine lipoarabinomannan tuberculosis assays in HIV-negative outpatients. *J. Clin.*

852      *Invest.* **130** (2020), doi:10.1172/jci140461.

853      62. K. Dijkman, C. C. Sombroek, R. A. W. Vervenne, S. O. Hofman, C. Boot, E. J. Remarque, C. H.  
854      M. Kocken, T. H. M. Ottenhoff, I. Kondova, M. A. Khayum, K. G. Haanstra, M. P. M. Vierboom,  
855      F. A. W. Verreck, Prevention of tuberculosis infection and disease by local BCG in repeatedly  
856      exposed rhesus macaques. *Nat. Med.* **25**, 255–262 (2019).

857      63. V. Balasubramanian, E. H. Wiegshaus, B. T. Taylor, D. W. Smith, Pathogenesis of tuberculosis:  
858      pathway to apical localization. *Tuber. Lung Dis.* **75** (1994), pp. 168–178.

859      64. S. R. Allie, J. E. Bradley, U. Mudunuru, M. D. Schultz, B. A. Graf, F. E. Lund, T. D. Randall, The  
860      establishment of resident memory B cells in the lung requires local antigen encounter. *Nat.*  
861      *Immunol.* **20**, 97–108 (2019).

862      65. T. Onodera, Y. Takahashi, Y. Yokoi, M. Ato, Y. Kodama, S. Hachimura, T. Kurosaki, K.  
863      Kobayashi, Memory B cells in the lung participate in protective humoral immune responses to  
864      pulmonary influenza virus reinfection. *Proc. Natl. Acad. Sci. U. S. A.* **109**, 2485–2490 (2012).

865      66. S. A. Schlottmann, N. Jain, N. Chirmule, M. T. Esser, A novel chemistry for conjugating  
866      pneumococcal polysaccharides to Luminex microspheres. *J. Immunol. Methods.* **309**, 75–85  
867      (2006).

868      67. E. van Woudenberg, E. B. Irvine, L. Davies, M. de Kock, W. A. Hanekom, C. L. Day, S. Fortune,  
869      G. Alter, HIV Is Associated with Modified Humoral Immune Responses in the Setting of HIV/TB  
870      Coinfection. *mSphere.* **5** (2020), doi:10.1128/mSphere.00104-20.

871      68. E. P. Brown, K. G. Dowell, A. W. Boesch, E. Normandin, A. E. Mahan, T. Chu, D. H. Barouch, C.  
872      Bailey-Kellogg, G. Alter, M. E. Ackerman, Multiplexed Fc array for evaluation of antigen-specific  
873      antibody effector profiles. *J. Immunol. Methods.* **443**, 33–44 (2017).

874      69. M. E. Ackerman, B. Moldt, R. T. Wyatt, A. S. Dugast, E. McAndrew, S. Tsoukas, S. Jost, C. T.  
875      Berger, G. Sciaranghella, Q. Liu, D. J. Irvine, D. R. Burton, G. Alter, A robust, high-throughput  
876      assay to determine the phagocytic activity of clinical antibody samples. *J. Immunol. Methods.* **366**,

877 8–19 (2011).

878 70. C. B. Karsten, N. Mehta, S. A. Shin, T. J. Diefenbach, M. D. Slein, W. Karpinski, E. B. Irvine, T.  
879 Broge, T. J. Suscovich, G. Alter, A versatile high-throughput assay to characterize antibody-  
880 mediated neutrophil phagocytosis. *J. Immunol. Methods.* **471**, 46–56 (2019).

881 71. F. Bunea, Y. She, H. Ombao, A. Gongvatana, K. Devlin, R. Cohen, Penalized least squares  
882 regression methods and applications to neuroimaging. *Neuroimage.* **55**, 1519–1527 (2011).

883

884

885

886

887

888

889

890

891

892

893

894

895

896

897

898

899

900

901

902 **Acknowledgements**

903 We thank the Vaccine research center at the National Institutes of Health for providing the rhesus macaque  
904 plasma and BAL samples from the BCG route vaccination study. We thank the Tulane National Primate  
905 Research Center for providing the rhesus macaque plasma samples from the attenuated *Mtb* (*Mtb*-Δ*sigH*)  
906 vaccination study. We thank the Harvard Medical School, Laboratory for Systems Pharmacology for  
907 allowing the use of their automated microscope.

908

909 **Funding**

910 Ragon Institute of MGH, MIT, and Harvard and the SAMANA Kay MGH Research Scholar Program.  
911 Bill and Melinda Gates Foundation: OPP1156795.  
912 Defense Advanced Research Projects Agency: W911NF-19-2-0017.  
913 National Institutes of Health: U54CA225088, U2CCA233262, U2CCA233280, AI150171-01, and  
914 Contract No. 75N93019C00071.

915

916 **Author Contributions**

917 E.B.I. – Conceptualization, Methodology, Software, Validation, Formal Analysis, Investigation, Data  
918 Curation, Writing Original Draft, Review and Editing, Visualization, Funding Acquisition; A.O. –  
919 Validation, Investigation, Review and Editing; P.A.D. – Conceptualization, Resources, Data Curation,  
920 Review and Editing; S.S. – Investigation, Review and Editing; A.C. – Methodology, Resources, Review  
921 and Editing; W.L. – Methodology, Review and Editing; W.H. – Validation, Investigation, Resources; S.M.  
922 – Conceptualization, Methodology, Resources, Review and Editing; D.K. – Conceptualization,  
923 Methodology, Resources, Data Curation, Review and Editing; H.P.G – Investigation, Resources, Data  
924 Curation; J.L.F. – Conceptualization, Methodology, Resources, Review and Editing, Supervision; M.R. –  
925 Conceptualization, Resources, Review and Editing, Supervision; R.A.S. – Conceptualization,  
926 Methodology, Resources, Review and Editing, Supervision; A.P. – Conceptualization, Methodology,

927 Resources, Review and Editing, Supervision; S.F. – Conceptualization, Methodology, Resources, Review  
928 and Editing, Supervision, Project Administration, Funding Acquisition; G.A. – Conceptualization,  
929 Methodology, Resources, Review and Editing, Supervision, Project Administration, Funding Acquisition.  
930

931 **Competing Interests**

932 Galit Alter is a founder of SeromYx Systems, Inc.  
933

934 **Data and materials availability**

935 All data associated with this study are available in the main text or in the supplementary materials. Any  
936 additional materials data, and code will be made available to members of the scientific community in a  
937 timely fashion following a reasonable request.  
938

939 **List of Supplementary Materials**

940 Figure S1: Antigen-specific Fc $\gamma$ R binding capacity of plasma and BAL antibodies  
941 Figure S2: Plasma IgG1 and IgA titers from the attenuated *Mtb* (*Mtb*-Δ*sigH*) vaccination cohort  
942 Data S1: Data\_SystemsSerology  
943 Code S1: Code\_LASSO\_PLSDA  
944

945

946

947

948

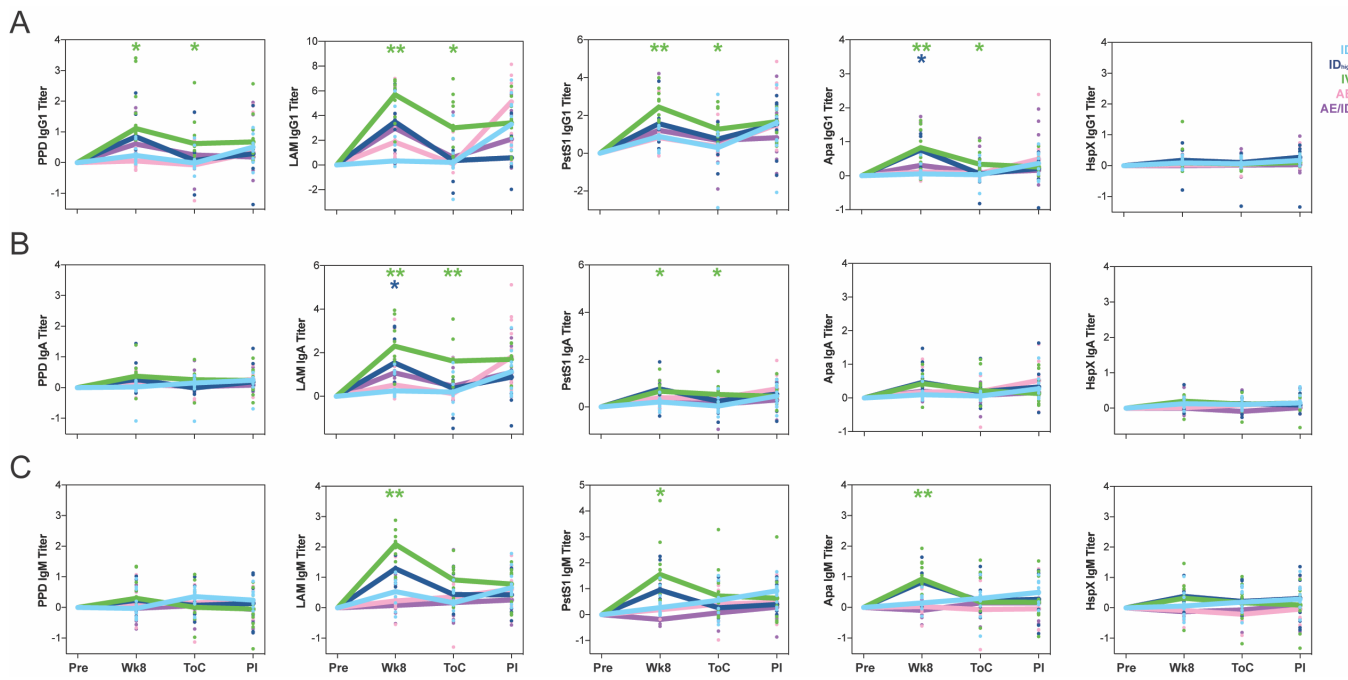
949

950

951

952

## FIGURES

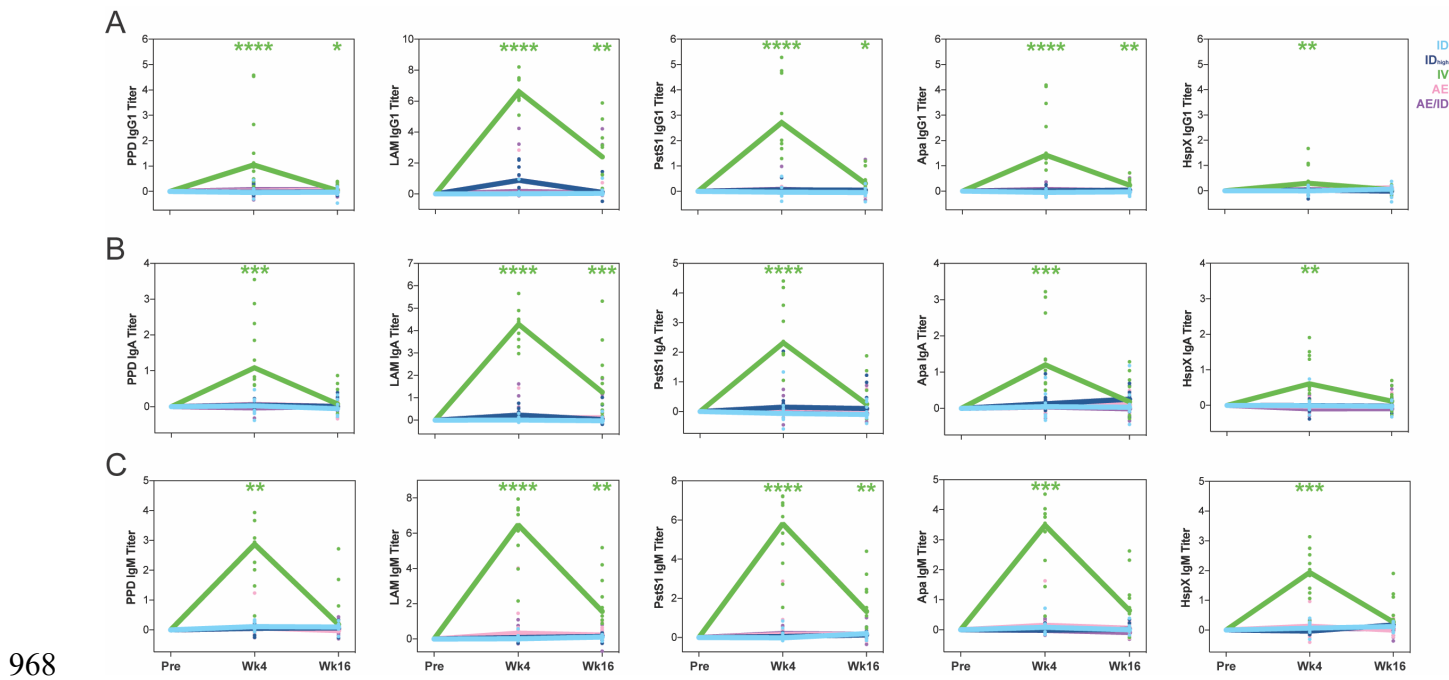


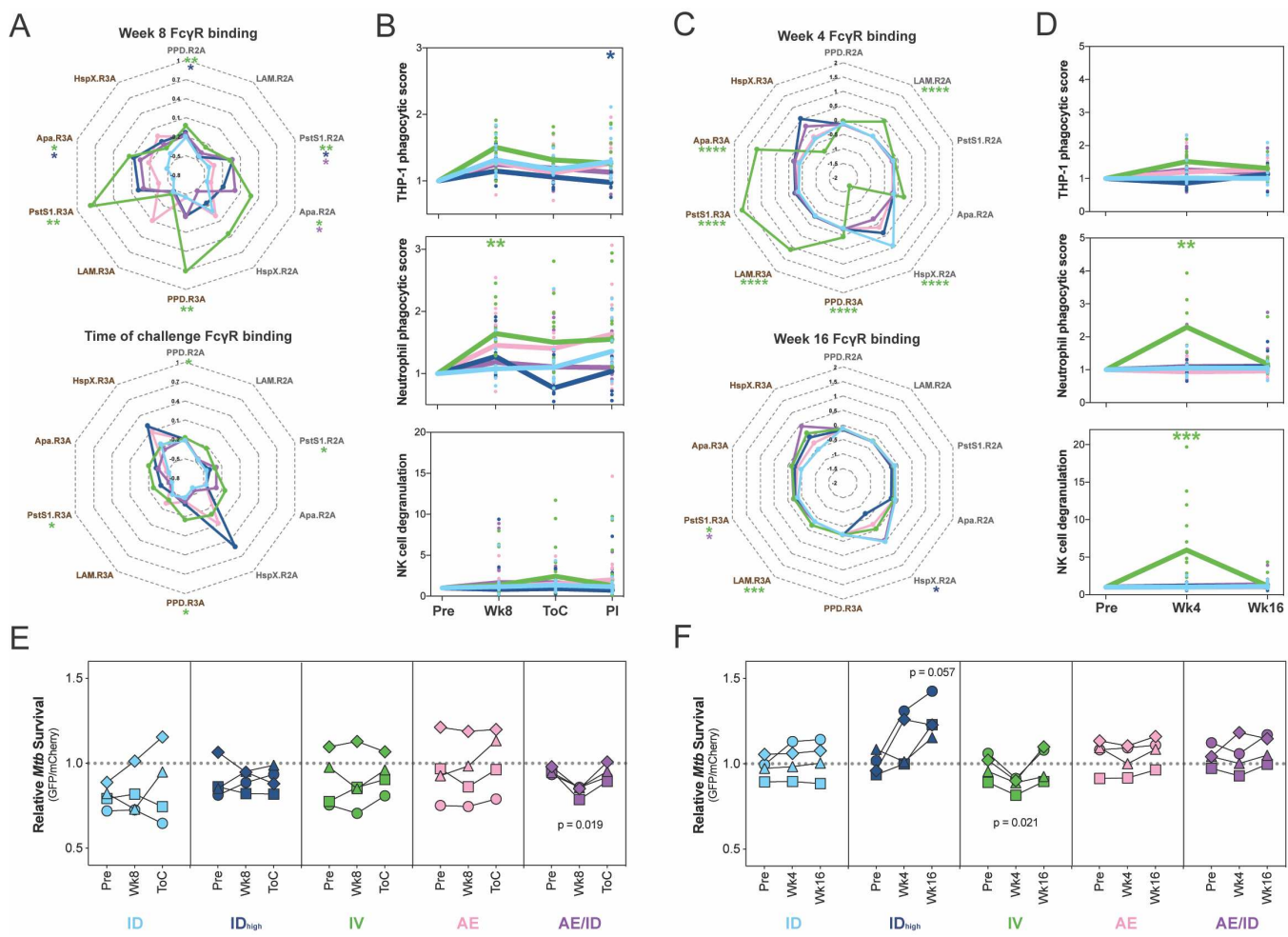
954 **Figure 1: IV BCG immunized primates exhibit higher and more durable plasma antibody titers.**

955 Fold change in (A) IgG1, (B) IgA, and (C) IgM titers present in the plasma of each rhesus macaque  
956 following BCG vaccination were determined via Luminex. Fold changes were calculated as fold change  
957 in Luminex median fluorescence intensity (MFI) over the pre-vaccination level for each primate. A base-  
958 2 log scale is used for the y-axis. Timepoints: pre-vaccination (Pre), week 8 post-BCG vaccination (Wk8),  
959 time of challenge at week 24 post-BCG vaccination (ToC), post-infection at week 28 post-BCG  
960 vaccination (PI). Groups: standard intradermal BCG (light blue), high intradermal BCG (dark blue),  
961 intravenous BCG (green), aerosol BCG (pink), aerosol + intradermal BCG (purple). Each dot represents  
962 a single animal at the respective timepoint. The lines represent group medians over time. Kruskal-Wallis  
963 with Dunn's multiple-comparison tests were performed on the fold change values at each timepoint,  
964 comparing each vaccination group to the standard intradermal BCG group. Adjusted p-values are as  
965 follows: \*, p < 0.05; \*\*, p < 0.01; \*\*\*, p < 0.001; \*\*\*\*, p < 0.0001.

966

967





984

985 **Figure 3: Antibodies from IV BCG vaccinated primates drive innate immune activation. (A and C)**

986 Radar plots of fold change in (A) plasma and (C) BAL antibody Fc $\gamma$ R binding activity of each group post-  
 987 BCG vaccination. Fold changes were calculated as fold change in Luminex MFI over the pre-vaccination  
 988 level for each primate. Median z-score of each group is plotted for a given feature. (B and D) Fold change  
 989 in (B) plasma and (D) BAL antibody-dependent cellular phagocytosis by THP-1 cells (top), antibody-  
 990 dependent neutrophil phagocytosis by primary human neutrophils (middle), antibody-dependent primary  
 991 human NK cell degranulation determined by % of cells CD107a positive (bottom). Fold changes were  
 992 calculated as fold change over the pre-vaccination level for each primate. Each dot represents a single  
 993 animal at the respective timepoint. The lines represent group medians over time. (E and F) *in vitro*  
 994 macrophage *Mtb* survival assay using pooled (E) plasma and (F) BAL from each vaccination group at  
 995 each timepoint. y-axis shows live (GFP) / total (mCherry) *Mtb* burden in human monocyte-derived

996 macrophages. Lower on the y-axis indicates increased intracellular *Mtb* killing in macrophages. Each set  
997 of connected dots indicates the activity of pools from different timepoints run across the same healthy  
998 human macrophage donor; 4 donors were run in total. Plasma timepoints: pre-vaccination (Pre), week 8  
999 post-BCG vaccination (Wk8), and time of challenge at week 24 post-BCG vaccination (ToC). BAL  
1000 timepoints: pre-vaccination (Pre), week 4 post-BCG vaccination (Wk4), week 16 post-BCG vaccination  
1001 (Wk16). Groups: standard intradermal BCG (light blue), high intradermal BCG (dark blue), intravenous  
1002 BCG (green), aerosol BCG (pink), aerosol + intradermal BCG (purple). **(A – D)** Kruskal-Wallis with  
1003 Dunn's multiple-comparison test was performed on the fold change values at each timepoint, comparing  
1004 each vaccination group to the standard intradermal BCG group. **(E and F)** Repeated measures ANOVA  
1005 with Dunnett's multiple comparisons test was performed for each vaccination group, comparing pre-  
1006 vaccination restrictive activity with that of each post-vaccination timepoint. Adjusted p-values are as  
1007 follows: \*, p < 0.05; \*\*, p < 0.01; \*\*\*, p < 0.001; \*\*\*\*, p < 0.0001.

1008

1009

1010

1011

1012

1013

1014

1015

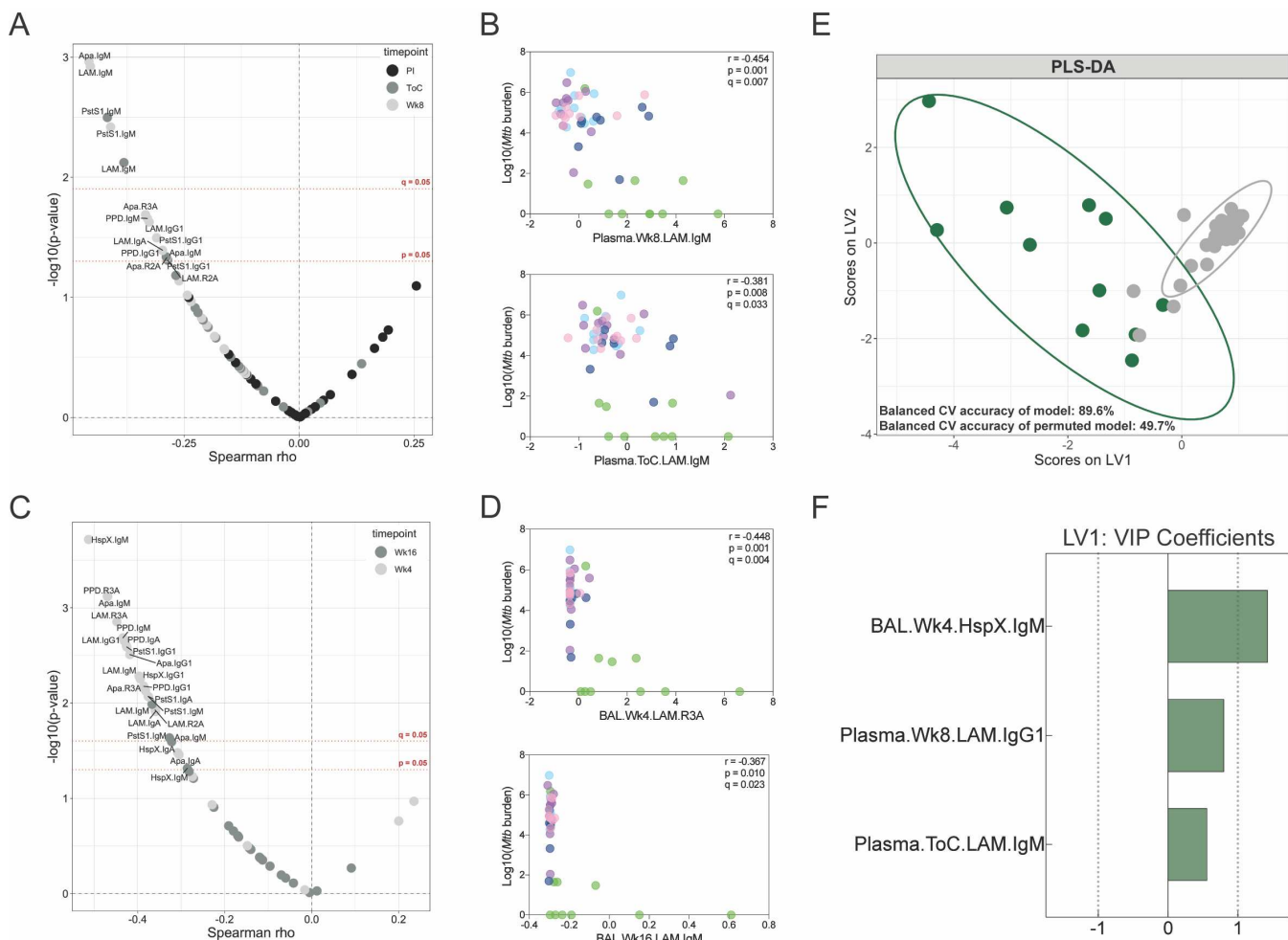
1016

1017

1018

1019

1020



1021

1022 **Figure 4: Numerous BCG-induced antibody features are associated with reduced *Mtb* burden. (A**  
 1023 **and C) Spearman correlations between base-10 log(*Mtb* burden) at necropsy and each (A) plasma and (C)**  
 1024 **BAL antibody measurement post-vaccination were computed. The x-axis indicates the spearman rho value**  
 1025 **associated with a given antibody feature. The y-axis indicates the negative base-10 log of the p-value**  
 1026 **associated with a given antibody feature. Antibody features are colored by their timepoint. (A) Plasma**  
 1027 **colors: week 8 post-BCG vaccination (light grey), time of challenge at week 24 post-BCG vaccination**  
 1028 **(dark grey), post-infection at week 28 post-BCG vaccination (black). (C) BAL colors: week 4 post-BCG**  
 1029 **vaccination (light grey), week 16 post-BCG vaccination (dark grey). (B and D) Spearman correlations**  
 1030 **between base-10 log(*Mtb* burden) at necropsy and select (B) plasma and (D) BAL antibody measurements.**  
 1031 **Points are colored by vaccination group: standard intradermal BCG (light blue), high intradermal BCG**  
 1032 **(dark blue), intravenous BCG (green), aerosol BCG (pink), aerosol + intradermal BCG (purple). Fold**

1033 change antibody measurements were subjected to a z-score transformation prior to correlation analyses.

1034 Adjusted p-values (q-values) computed by the Benjamini-Hochberg procedure. (**E and F**) PLS-DA model

1035 fit using the antibody features selected by LASSO regularization. (**E**) Graph of the first two latent variables

1036 (LVs) of the model. Protected primates (green) had an *Mtb* burden < 1000 at necropsy. Susceptible

1037 primates (grey) had an *Mtb* burden > 1000 at necropsy. Ellipses show 95% confidence intervals. Balanced

1038 cross-validation (CV) accuracy of the model and permuted model are indicated. Accuracy of model is

1039 significantly higher than that of the permuted model (Mann-Whitney U test,  $p < 2.2e^{-16}$ ). (**F**) Variable

1040 importance in the projection (VIP) coefficients on LV1 for each model feature, indicating the extent to

1041 which each feature contributes to separation along LV1.

1042

1043

1044

1045

1046

1047

1048

1049

1050

1051

1052

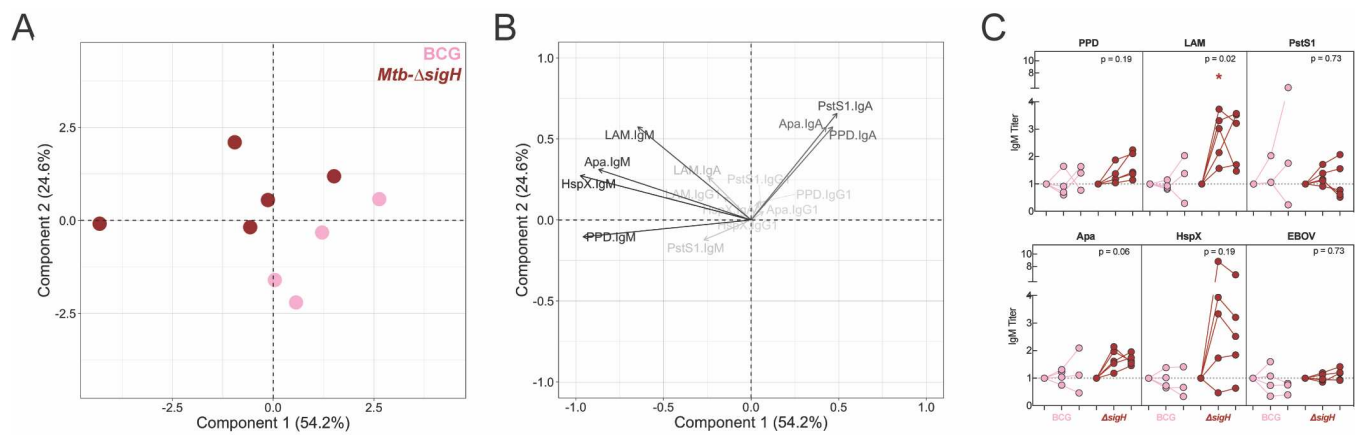
1053

1054

1055

1056

1057



1058

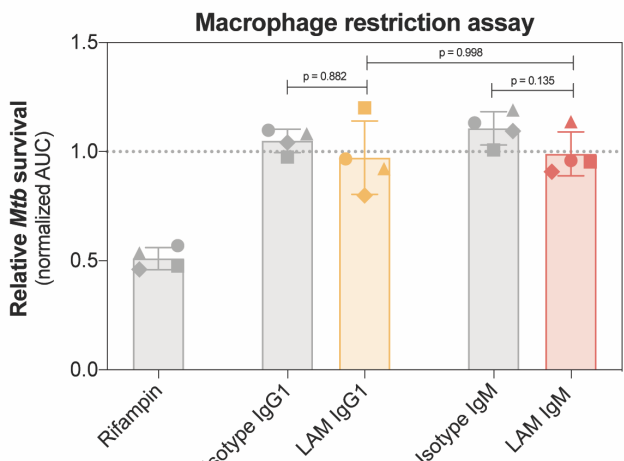
1059 **Figure 5: Protective vaccination with attenuated *Mtb* (*Mtb*- $\Delta$ *sigH*) is associated with increased**  
1060 **plasma IgM titers. (A and B)** Principal component analysis using fold change IgG1, IgA, and IgM titers  
1061 measured at week 7 post-vaccination in an attenuated *Mtb* rhesus macaque vaccination cohort. Fold  
1062 changes were calculated as fold change in Luminex MFI over the pre-vaccination level for each primate.  
1063 Fold change antibody measurements were subjected to a z-score transformation prior to principal  
1064 component analysis. **(A)** Score plot. Aerosol *Mtb*- $\Delta$ *sigH* vaccination group (red), aerosol BCG vaccination  
1065 group (pink). **(B)** Loading plot. Relative contribution of variables to the components are indicated by a  
1066 color gradient. Light grey variables contribute least, black variables contribute most. **(C)** Fold change in  
1067 IgM titer present in the plasma of each rhesus macaque following vaccination determined via Luminex.  
1068 Fold changes were calculated as fold change in Luminex MFI over the pre-vaccination level for each  
1069 primate. Each dot represents a single animal at the respective timepoint. Timepoints: pre-vaccination  
1070 (left), week 7 post-vaccination (middle), week 15 post-vaccination at necropsy (right). *Mtb* challenge was  
1071 performed week 8 post-vaccination. Mann-Whitney U test was performed on the fold change values at  
1072 each timepoint, comparing aerosol *Mtb*- $\Delta$ *sigH* to the aerosol BCG group. p-values are as follows: \*, p <  
1073 0.05; \*\*, p < 0.01; \*\*\*, p < 0.001; \*\*\*\*, p < 0.0001.

1074

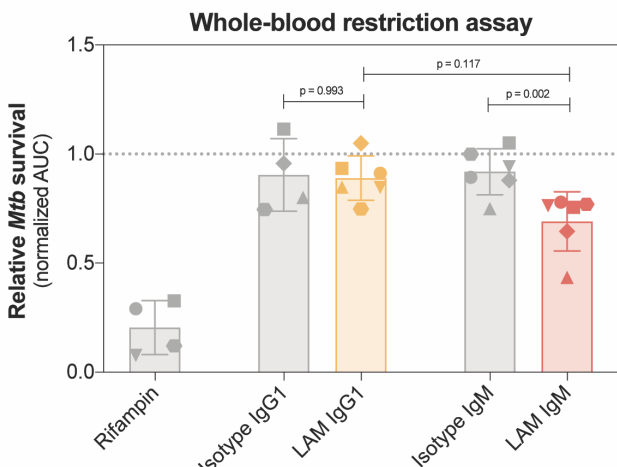
1075

1076

1077 A



1077 B



1078 **Figure 6: LAM IgM monoclonal antibody drives superior *Mtb* restriction in human whole-blood.**

1079 (A) Macrophage restriction assay. Each antibody was added (final concentration 50 $\mu$ g/mL) to human  
1080 monocyte-derived macrophages infected with a luminescent *Mtb* reporter strain (*Mtb*-276). Growth curves  
1081 in the presence of each antibody treatment were generated by taking luminescence readings every 24 hours  
1082 up to 120 hours. Y-axis is the area under the *Mtb* growth curve normalized by the no antibody condition  
1083 of each donor. Each dot is the triplicate average from 1 donor. (B) Whole-blood restriction assay. Each  
1084 antibody (final concentration 25 $\mu$ g/mL) was tested for their ability to drive *Mtb* restriction in the context  
1085 of fresh human whole-blood using *Mtb*-276. Y-axis is the area under the *Mtb* growth curve, normalized  
1086 by the no antibody condition. Growth curves were generated by taking luminescence readings every 24  
1087 hours up to 120 hours. Each dot is the triplicate average from 1 donor. Repeated measures ANOVA with  
1088 Sidak's multiple comparisons test.